

Solid-State $^{79/81}\text{Br}$ NMR and Gauge-Including Projector-Augmented Wave Study of Structure, Symmetry, and Hydration State in Alkaline Earth Metal Bromides

Cory M. Widdifield and David L. Bryce*

Department of Chemistry and Centre for Catalysis Research and Innovation, University of Ottawa, 10 Marie Curie Pvt., Ottawa, Ontario, Canada

Received: September 21, 2009; Revised Manuscript Received: December 1, 2009

Bromine-79/81 solid-state NMR (SSNMR) spectroscopy is established as a tool to characterize the local structure and symmetry about bromide ions in inorganic systems. Benchmark experimental $^{79/81}\text{Br}$ SSNMR data are acquired for CaBr_2 , SrBr_2 , BaBr_2 , $\text{MgBr}_2 \cdot 6\text{H}_2\text{O}$, $\text{SrBr}_2 \cdot 6\text{H}_2\text{O}$, $\text{BaBr}_2 \cdot 2\text{H}_2\text{O}$, and $\text{CaBr}_2 \cdot x\text{H}_2\text{O}$ using the Solomon echo and/or QCPMG pulse sequences in magnetic fields of 11.75 and 21.1 T. Analytical line-shape analysis provides $^{79/81}\text{Br}$ electric field gradient (EFG) tensor parameters (including ^{79}Br quadrupolar coupling constants, $C_Q(^{79}\text{Br})$, of up to 75.1(5) MHz in CaBr_2), chemical shift tensor parameters (including the largest reported anisotropy), and the relative orientation of the tensor principal axis systems. These data are interpreted in terms of structure and symmetry. Our results indicate that ionic bromide systems should be generally accessible to characterization by $^{79/81}\text{Br}$ SSNMR despite sizable quadrupolar interactions. The resolving capabilities of $^{79/81}\text{Br}$ SSNMR spectroscopy are illustrated, using samples which possess up to four magnetically inequivalent sites, and through a rare example of ^{79}Br magic-angle spinning NMR for a Br in a noncubic lattice. Bromine-79/81 SSNMR spectroscopy is demonstrated to be sensitive to the presence of hydrates (i.e., pseudopolymorphism), via drastic changes in C_Q and δ_{iso} . The changes are diagnostic to an extent that the composition of the mixture $\text{CaBr}_2 \cdot x\text{H}_2\text{O}$ is determined for the first time. This technique should therefore be applicable to characterize other unknown mixtures or polymorphs. Important instances where ^{79}Br nuclear quadrupole resonance data were found to be deficient are noted and corrected. GIPAW DFT computations are shown to be generally in very good agreement with the experimental $^{79/81}\text{Br}$ SSNMR observations. Finally, it is demonstrated that the origin of the EFG at the Br nuclei cannot be described quantitatively using a point charge model, even after including Sternheimer antishielding effects.

Introduction

Bromine is found naturally in seawater, brines, and various bromide salts.¹ In addition to their ubiquitous presence in synthetic organic chemistry, organic bromine-containing materials are applied as flame retardants, dyes, drilling fluids, fuel additives, nematocides, and fumigants. Silver bromide is the most commonly applied inorganic bromide-containing compound, primarily in photography. Recent evidence suggests that there is a negative environmental impact associated with using select bromine-containing materials, and their future use is being reduced.² Similarly, a recent editorial has noted the negative effects that halides have during the production of biomass fuels, as they corrode the steam lines of production facilities.³ In light of these accounts, methods must be further developed to (i) quantify the presence of bromine and bromides and (ii) comment upon bromine/bromide chemical environments. Our recent communication highlighted the pronounced sensitivity of $^{79/81}\text{Br}$ solid-state nuclear magnetic resonance (SSNMR) line shapes to the local environment about the bromide ions in MgBr_2 .⁴ Here, we establish and demonstrate the power of $^{79/81}\text{Br}$ SSNMR in the characterization and understanding of bromide-containing systems, with particular emphasis on the extraction of structural information.

Both naturally occurring isotopes of bromine (^{79}Br and ^{81}Br) possess NMR-active quadrupolar nuclei (i.e., $I > 1/2$) and are

present in high natural abundance (~50%). However, recent literature reviews report that $^{79/81}\text{Br}$ SSNMR data are sparse.^{5,6} Considering the relatively large nuclear electric quadrupole moments (Q)⁷ and Sternheimer antishielding factors^{8,9} possessed by the $^{79/81}\text{Br}$ nuclei, it is clear why $^{79/81}\text{Br}$ SSNMR spectroscopy is underdeveloped. When quadrupolar nuclei experience a nonzero electric field gradient (EFG), the EFG will couple with Q , which is known as the quadrupolar interaction (QI). This in turn leads to substantial SSNMR line-shape broadening in powdered samples, often to the extent that the SSNMR signal cannot be detected.

Most $^{79/81}\text{Br}$ SSNMR literature accounts involve alkali metal bromides or other cubic salts (such as AgBr , CuBr , and TlBr), as the QI at the bromine is zero by symmetry, thus rendering spectral acquisition straightforward.^{10–16} Over the past 20 years, few $^{79/81}\text{Br}$ SSNMR studies have been carried out on systems where the bromide experiences a small but nonzero QI. For example, studies on microcrystalline samples include perbromates,^{17–20} oxygen-doped BaFBr ,²¹ and bromide-containing sodalites.^{22–25} Studies using single crystals have characterized bromide environments with more substantial QIs, such as in $\text{K}_2\text{Pt}(\text{CN})_4\text{Br}_{0.3} \cdot 3.2\text{H}_2\text{O}$,^{26,27} tris-sarcosine CaBr_2 ,^{28,29} and deuterated glycyl-L-alanine $\text{HBr} \cdot \text{H}_2\text{O}$.³⁰ Recently, the “STREAQI” method was applied to measure the bromine QIs in L-leucine HBr and L-tyrosine HBr ,³¹ and ^{14}N and ^{81}Br SSNMR was used to study several polycrystalline $\text{C}_x\text{H}_{2x+1}(\text{CH}_3)_3\text{NBr}$ samples.³²

Current reviews pertaining to the NMR-active quadrupolar halogen nuclides^{5,6,33} underscore the significant ongoing ad-

* Author to whom correspondence is to be addressed. Tel: +1 613 562 5800 ext 2018. Fax: +1 613 562 5170. E-mail: dbryce@uottawa.ca.

vances in $^{35/37}\text{Cl}$ SSNMR spectroscopy. Recent progress is primarily due to the increasing availability of ultrahigh magnetic fields (i.e., $\mathbf{B}_0 > 18.8$ T) and the development of advanced pulse sequences.^{34–41} Prior to these developments, $^{35/37}\text{Cl}$ SSNMR studies were limited to systems where the chlorine environment was known to be nearly octahedral or tetrahedral.^{14,42–50} Hence, the systems traditionally investigated using $^{35/37}\text{Cl}$ SSNMR were similar to those previously studied using $^{79/81}\text{Br}$ SSNMR. In the past five years, new insight into the relationship between $^{35/37}\text{Cl}$ SSNMR parameters and local molecular and electronic structure has been obtained for a range of interesting compounds, including amino acid hydrochlorides,^{51–54} alkaline earth metal chlorides,^{55,56} hydrochloride pharmaceuticals,⁵⁷ group 4 organometallic chlorides,⁵⁸ and halide-containing ionic liquids.⁵⁹ Most of these recent studies featured chlorides that were not present at a position of high symmetry; hence, these characterizations were made for systems where the QI is nonzero. We believe that $^{79/81}\text{Br}$ SSNMR may be developed in a similar fashion.

To provide an experimental basis for understanding the relationship between local structure and symmetry at the bromine and observable $^{79/81}\text{Br}$ SSNMR parameters, we present a systematic $^{79/81}\text{Br}$ SSNMR study of several alkaline earth metal bromides and corresponding stable hydrates. While these systems possess relatively simple structures, a variety of Br environments are represented. These compounds (i) contain different numbers of magnetically unique bromide sites, ranging from 1 to 4, (ii) exhibit distinct Br QIs, both in terms of magnitude and symmetry, and (iii) form stable hydrates, thus allowing for an investigation of the relationship between pseudopolymorphism and $^{79/81}\text{Br}$ SSNMR parameters. These systems are also more than academically interesting: CaBr_2 is used in oil drilling brine solutions, as a desiccant, a food preservative, and fire retardant. Eu(III)-doped CaBr_2 -based aluminoborate glasses are candidate materials for use in lasers, optical amplifiers, and optical storage devices.⁶⁰ Strontium bromide has been used as a vapor-phase laser.⁶¹ BaBr_2 single-crystals are excellent X-ray storage phosphors when doped with lanthanide ions such as Eu(II)⁶² or Ce(III)⁶³ and have recently been proposed for use in X- and γ -ray scintillation applications.^{64,65} By combining multiple field $^{79/81}\text{Br}$ SSNMR experiments with gauge-including projector-augmented wave (GIPAW) density functional theory (DFT) quantum chemical computations, we show that significant insight is available regarding the bromide environments in the alkaline earth metal bromides and corresponding hydrates. It will also be shown that pseudopolymorphs are easily distinguished and characterized, and that the composition of a simple mixture may be determined using $^{79/81}\text{Br}$ SSNMR experiments.

Solid-State NMR: Observable Parameters

The NMR spectra discussed here are modeled using analytical simulations⁶⁶ which include line-shape contributions from the QI and chemical shift anisotropy (CSA). Other contributions are negligible.

1. The Nuclear Electric Quadrupole Interaction. For the systems considered here, the two satellite transitions (ST, $m_l = \pm 3/2 \leftrightarrow \pm 1/2$) are either beneath our detection limits or are excessively time-consuming to collect. The observed SSNMR signals correspond only to the central transition (CT, $m_l = +1/2 \leftrightarrow -1/2$).

The EFG is described using a traceless, symmetric second-rank tensor ($\ddot{\mathcal{V}}$). In its own principal axis system (PAS), $\ddot{\mathcal{V}}$ may be represented using a diagonal 3×3 Cartesian matrix. The

diagonal elements are known as the principal components (V_{ii}) and are defined such that $|V_{11}| \leq |V_{22}| \leq |V_{33}|$. The nuclear quadrupole coupling constant (C_Q) and asymmetry parameter (η_Q) are related to the principal components: $C_Q = eQV_{33}/h$; $\eta_Q = (V_{11} - V_{22})/V_{33}$, where C_Q is in frequency units, and η_Q is unitless and ranges between 0 and 1.

2. Magnetic Shielding Anisotropy. Magnetic shielding may be described using a symmetric second-rank tensor ($\ddot{\sigma}$) with a trace (the isotropic magnetic shielding value, σ_{iso}). In its own PAS, $\ddot{\sigma}$ is specified using three principal components (σ_{ii}), such that $\sigma_{11} \leq \sigma_{22} \leq \sigma_{33}$. According to the Maryland convention,^{67,68} $\ddot{\sigma}$ may be described by the following parameters: $\sigma_{\text{iso}} = (\sigma_{11} + \sigma_{22} + \sigma_{33})/3$; $\Omega = \sigma_{33} - \sigma_{11}$ (the span); $\kappa = 3(\sigma_{\text{iso}} - \sigma_{22})/\Omega$, where σ_{iso} is in ppm, Ω is in ppm and takes a positive value, and κ is unitless, ranging from -1 to $+1$.

The $\ddot{\sigma}$ tensor is not measured experimentally in solid samples; rather, the chemical shift tensor ($\ddot{\delta}$) is measured. The elements of $\ddot{\sigma}$ (σ_{ij}) may be related to $\ddot{\delta}$ elements (δ_{ij}):

$$\delta_{ij} = \frac{\sigma_{\text{ref},\text{iso}} - \sigma_{ij}}{1 - \sigma_{\text{ref},\text{iso}}} \quad (1.1)$$

where $\sigma_{\text{ref},\text{iso}}$ is a reference shielding value. Hence, $\ddot{\sigma}$ tensor parameters can be transformed into equivalent expressions which parametrize $\ddot{\delta}$ (in the $\ddot{\delta}$ PAS, $\delta_{11} \geq \delta_{22} \geq \delta_{33}$): $\delta_{\text{iso}} = (1/3)(\delta_{11} + \delta_{22} + \delta_{33})$, $\Omega = (\delta_{11} - \delta_{33})(1 - \sigma_{\text{ref},\text{iso}}) \approx (\delta_{11} - \delta_{33})$, $\kappa \equiv 3(\delta_{22} - \delta_{\text{iso}})/(\delta_{11} - \delta_{33}) \approx 3(\delta_{22} - \delta_{\text{iso}})/\Omega$, where the approximate versions of Ω and κ are valid in the present study and generally when $1 - \sigma_{\text{ref},\text{iso}} \approx 1$.⁶⁹

When effects due to both the QI and CSA are observed, it may be possible to determine the relative orientation of the $\ddot{\mathcal{V}}$ and $\ddot{\sigma}$ PASs.⁷⁰ Three Euler angles (α , β , and γ) describe the relative orientation. Further information pertaining to Euler angle conventions may be found in ref 70. As the magnetic shielding and QI each possess a different \mathbf{B}_0 dependence, one approach to improve the precision of the measurement is to acquire data at two different applied fields. As bromine offers two NMR-active isotopes, experiments on both isotopes at two different fields can be thought of as collecting data at four different applied fields.

Experimental Section

1. Sample Preparation. CaBr_2 (99.98%), SrBr_2 (99.995%), and BaBr_2 (99.999%) were purchased from Aldrich as anhydrous beads. All these compounds are hygroscopic and were stored and prepared for use under either dry N_2 or Ar. $\text{MgBr}_2 \cdot 6\text{H}_2\text{O}$ (99%), $\text{SrBr}_2 \cdot 6\text{H}_2\text{O}$ (99%), and $\text{CaBr}_2 \cdot x\text{H}_2\text{O}$ (98%) were purchased from Aldrich in either polycrystalline or microcrystalline powder form. $\text{BaBr}_2 \cdot 2\text{H}_2\text{O}$ (99.3%) was purchased from Alfa Aesar as a microcrystalline powder. All hydrates are air stable. For all $^{79/81}\text{Br}$ SSNMR experiments, samples were powdered and tightly packed into 4 mm o.d. Bruker magic-angle spinning (MAS) zirconia rotors.

2. Solid-State NMR. Bromine-79/81 SSNMR data were acquired at the University of Ottawa using a Bruker Avance spectrometer operating at $\mathbf{B}_0 = 11.75$ T ($\nu_0(^1\text{H}) = 500.13$ MHz) and at the National Ultrahigh-field NMR Facility for Solids in Ottawa using a Bruker AvanceII spectrometer operating at $\mathbf{B}_0 = 21.1$ T ($\nu_0(^1\text{H}) = 900.08$ MHz). At 11.75 T, all experiments used a Bruker 4 mm HXY MAS probe ($\nu_0(^{81}\text{Br}) = 135.076$ MHz; $\nu_0(^{79}\text{Br}) = 125.310$ MHz). At 21.1 T, experiments performed on stationary samples used a Bruker 4 mm HX MAS probe ($\nu_0(^{81}\text{Br}) = 243.093$ MHz; $\nu_0(^{79}\text{Br}) = 225.519$ MHz),

while MAS experiments on $\text{BaBr}_2 \cdot 2\text{H}_2\text{O}$ used Bruker 3.2 mm and 2.5 mm HX MAS probes for the detection of ^{81}Br and ^{79}Br SSNMR signals, respectively. Due to the known heating effect of MAS on the sample, and as the loss of H_2O in powdered $\text{BaBr}_2 \cdot 2\text{H}_2\text{O}$ occurs upon heating above 323 K,⁷¹ all MAS experiments were carried out while passing cooled N_2 gas through the probes. Bromine chemical shifts and $\pi/2$ pulse widths were determined using the $^{79/81}\text{Br}$ NMR signals of KBr powder ($\delta_{\text{iso}}(\text{KBr}(\text{s})) = 0.0$ ppm). As the KBr ion lattice is cubic, the CT-selective (i.e., “solid $\pi/2$ ”) pulse widths used for the alkaline earth metal bromides were scaled by $1/(I + 1/2) = 1/2$. Bromine-79/81 SSNMR signals were primarily acquired using the Solomon echo (i.e., $\pi/2 - \tau_1 - \pi/2 - \tau_2 - acq$) pulse sequence^{72,73} with the phase cycling of Kunwar et al.⁷⁴ For all samples except $\text{BaBr}_2 \cdot 2\text{H}_2\text{O}$ and $\text{SrBr}_2 \cdot 6\text{H}_2\text{O}$, long T_2 values (estimated using the quadrupolar Carr–Purcell–Meiboom–Gill (QCPMG) pulse sequence, *vide infra*) allowed for whole echo data acquisition, thus increasing the S/N ratio of the echo experiment by $\sqrt{2}$. Typical $^{79/81}\text{Br}$ Solomon echo parameters (for full details, see Supporting Information, Table S1) were the following: $\pi/2 = 1.0$ to $3.0 \mu\text{s}$, spectral window = 250 to 2000 kHz, $\tau_1 = 100$ to $500 \mu\text{s}$ (whole echo) or 26 to $100 \mu\text{s}$ (half echo), pulse delay = 0.3 to 0.8 s, collection of 1024 to 4096 data points per transient and 1000 to 64k transients. MAS NMR data were acquired under rotor-synchronized conditions. The QCPMG pulse sequence^{39,75,76} was used at $\mathbf{B}_0 = 11.75$ T to enhance the $^{79/81}\text{Br}$ SSNMR signals and thus reduce experiment times. For typical QCPMG parameters, see Table S1. For all hydrates, the effect of continuous wave ^1H decoupling was tested. Typical $\nu_{\text{rf}}(^1\text{H})$ values were 40 to 100 kHz.

For most of the samples studied, variable offset cumulative spectrum (VOCS) data acquisition methods were used to observe the very broad $^{79/81}\text{Br}$ CT NMR signals.^{77–79} Offsets varied from 200 to 400 kHz for Solomon echo experiments and from 86.31 to 95.90 kHz for QCPMG experiments. Each component spectrum (“subspectrum”) was processed normally and then combined in the frequency-domain by coaddition.

3. GIPAW DFT Computations. GIPAW DFT computations were carried out using version 4.1 of CASTEP-NMR,^{80–83} using input files generated from Materials Studio 3.2. Bromine on-the-fly pseudopotential files were obtained directly from Accelrys Inc. (San Diego, CA). Geometry optimizations, as well as NMR calculations (i.e., of the $\ddot{\mathcal{V}}$ and $\ddot{\sigma}$ tensors), used the PBE exchange-correlation (XC) functional,^{84,85} under the generalized gradient approximation (GGA). Additional NMR computations employed the PW91 XC functional^{86–90} and yielded similar computed values to the PBE calculations. NMR parameter convergence was tested by varying both the Monkhorst–Pack⁹¹ k -point sampling of the Brillouin zone and the plane wave basis set energy cutoff (E_{cut}). All NMR calculations used the ‘precise’ setting, as defined by Materials Studio, for the fast-Fourier transform (FFT) grid, except $\text{MgBr}_2 \cdot 6\text{H}_2\text{O}$, where the ‘standard’ FFT grid setting was used due to computational resource limitations. All geometry optimizations used the ‘standard’ FFT grid setting. Conversion of calculated σ_{ij} to δ_{ij} used the following procedure: the bromine σ_{iso} value for the reference compound KBr ($\sigma_{\text{iso,ref}}$) was computed using $E_{\text{cut}} = 800$ eV, a $6 \times 6 \times 6$ k -point grid, and the same XC functional as for the sample. This was followed by application of eq 1.1. The E_{cut} and k -point grid used for each system are in the footnotes to Tables 3 and 4. Computed energies, structure references, and additional computational input details are in Table S2, Supporting Information. Crystal structure

parameters used for NMR computations are in Table S3, Supporting Information.

For $\text{MgBr}_2 \cdot 6\text{H}_2\text{O}$ and $\text{SrBr}_2 \cdot 6\text{H}_2\text{O}$, two structural models were used for subsequent NMR computations, labeled as ‘model A’ and ‘model B’. For $\text{MgBr}_2 \cdot 6\text{H}_2\text{O}$, model A, the heavy atom positions of Andress and Gundermann⁹² and unit cell of Sorrell and Ramey⁹³ were used. Hydrogen atoms were added in Gaussview 3.0 and optimized using CASTEP. For model B, the heavy atom positions were adjusted slightly, while still remaining within the error bounds reported in the original paper. For $\text{SrBr}_2 \cdot 6\text{H}_2\text{O}$, model A, the heavy atom positions and unit cell of Abrahams and Vordemvenne were used.⁹⁴ Hydrogen positions were initially placed according to those of $\text{SrCl}_2 \cdot 6\text{H}_2\text{O}$,⁹⁵ as that structure was determined using neutron diffraction and should be isomorphic to $\text{SrBr}_2 \cdot 6\text{H}_2\text{O}$. The hydrogen positions were then optimized computationally. For model B, the procedure used was nearly identical, but the c unit cell positions of the Br were changed to $-c$, to agree with the halogen atom positions in the isomorphic $\text{SrCl}_2 \cdot 6\text{H}_2\text{O}$, $\text{CaBr}_2 \cdot 6\text{H}_2\text{O}$, and $\text{CaCl}_2 \cdot 6\text{H}_2\text{O}$ compounds.⁹⁶ After computational optimization of the hydrogen positions, NMR calculations were performed.

4. Point Charge Model Calculations. Calculations were semiautomated with Microsoft Excel, using full integer charges for the ions in the lattice. For all anhydrous compounds, point charge lattices corresponded to an $8 \times 8 \times 8$ super cell (except for SrBr_2 , where a $6 \times 6 \times 6$ super cell was used). This corresponds to 3435, 6792, and 6143 point charges and super cell volumes of 100.57 nm^3 , 208.77 nm^3 , and 208.30 nm^3 for CaBr_2 , SrBr_2 , and BaBr_2 , respectively. Calculations included Sternheimer antishielding effects, using $(1 - \gamma_{\infty}) = 80$.⁹⁷ To assess the influence of ionic charge on $C_Q(^{81}\text{Br})$, $q(\text{Ca})$ and $q(\text{Br})$ for CaBr_2 were varied.

Results and Discussion

1. Bromine-79/81 SSNMR Experiments.

A. Anhydrous Alkaline Earth Metal Bromides. The measured $^{79/81}\text{Br}$ NMR parameters for the anhydrous alkaline earth metal bromides CaBr_2 , SrBr_2 , and BaBr_2 are presented in Table 1.

i. CaBr_2 : An Example of Significant Bromine QI and CSA. Static $^{79/81}\text{Br}$ SSNMR spectra acquired at $\mathbf{B}_0 = 21.1$ T are broadened due to a nonzero EFG at the bromine, as the spectra span several MHz and feature line shapes that are characteristic of second-order quadrupolar broadening (Figure 1). While the $^{79/81}\text{Br}$ SSNMR signals are distributed over a large frequency range, they were acquired using the Solomon echo pulse sequence⁷² and VOCS data acquisition methods in about 8 h. Data acquisition was facilitated by efficient $^{79/81}\text{Br}$ quadrupolar T_1 relaxation.⁹⁸ A ^{81}Br SSNMR spectrum of CaBr_2 was acquired at 11.75 T under static conditions (see Figure S1, Supporting Information); however, the QCPMG pulse sequence and about two days of experiment time were required in order to obtain a spectrum with a reasonable S/N ratio (74 subspectra).

The ambient pressure and temperature structure of CaBr_2 is isomorphic to CaCl_2 ⁹⁹ and belongs to the orthorhombic $Pnnm$ space group.^{100,101} The bromide ions are located at m symmetry sites and coordinate to three Ca^{2+} ions in a distorted trigonal planar fashion (Figure 2a). Calcium-43 MAS SSNMR measurements exist for this compound,¹⁰⁴ and while ^{79}Br nuclear quadrupole resonance (NQR) data collected at 300 K determined a quadrupolar frequency (ν_Q) of 38.76 MHz,¹⁰⁵ insight into the $\ddot{\mathcal{V}}$ tensor symmetry or the $\ddot{\sigma}$ tensor was not obtained, as standard ^{79}Br NQR experiments are insensitive to these properties.

TABLE 1: Experimental $^{79/81}\text{Br}$ EFG and Chemical Shift Tensor Parameters: Anhydrous Alkaline Earth Metal Bromides^a

compound	site label	$ C_Q(^{81}\text{Br}) /\text{MHz}^b$	$ C_Q(^{79}\text{Br}) /\text{MHz}$	η_Q	$\delta_{\text{iso}}/\text{ppm}$	Ω/ppm	κ	α/deg	β/deg	γ/deg	$\nu_Q(^{79}\text{Br})/\text{MHz}^c$	
CaBr ₂	—	62.8(4)	75.1(5)	0.445(20)	280(50)	250(150)	0 ^d	270 ^d	90(20)	180 ^d	38.76(0.08)	
SrBr ₂	Br(1)	10.3(3)	12.3(3)	0.07(4)	422(5)	50(20)	-1 ^e	90 ^d	90(15)	180(5)	—	
	Br(2)	18.10(20)	21.65(20)	0.03(2)	410(8)	85(25)	-1 ^e	90 ^d	90(10)	180(8)	—	
	Br(3)	25.6(2)	30.6(2)	0.695(15)	320(10)	110(30)	0.3(4)	42(8)	90(10)	235(20)	16.54(0.10)	
	Br(4)	53.7(6)	64.2(6)	0.33(2)	300(50)	—	—	—	—	—	32.90(0.12)	
	BaBr ₂	Br(1)	23.5(3)	28.1(4)	0.17(2)	280(10)	200(20)	-0.6(2)	0 ^d	47(7)	180 ^d	13.96(0.3)/23.36(0.35)
	Br(2)	27.2(3)	32.5(3)	0.070(15)	480(15)	170(30)	0.1(2)	180 ^d	18(7)	180 ^d	—	

^a Error bounds are in parentheses. Parameter definitions are in the main text. ^b Although C_Q may take any real value, $|C_Q|$ is measured using SSNMR experiments. ^c From literature.¹⁰⁵ All ^{79}Br NQR measurements occurred at $T = 300$ K, except for BaBr₂, which was at $T = 209$ K.

^d Simulated NMR line-shape is insensitive to parameter variation. The value is assigned based on computational results. ^e Assumed based on crystallographic site symmetry.

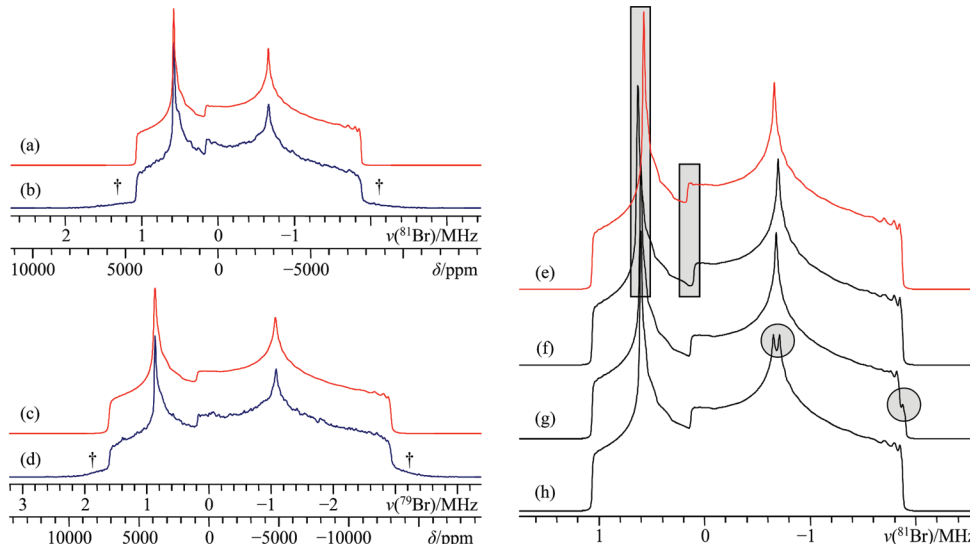


Figure 1. Analytical simulations (a, c), and experimental static VOCS Solomon echo (b, d) $^{79/81}\text{Br}$ SSNMR spectra of powdered CaBr₂, acquired at $B_0 = 21.1$ T. Partially excited ST are denoted using “†”. To illustrate the necessity of considering the effects of noncoincident \vec{V} and $\vec{\sigma}$ tensor frames, analytical simulations are provided using identical values as the best fit simulation (e) except (f) $\beta = 0^\circ$, (g) $\beta = 45^\circ$, (h) $\beta = 45^\circ$ and $\alpha = 0^\circ$. In each case (f–h), there exists additional fine structure (highlighted regions), which disagree with the best fit spectrum.

The measured values of $C_Q(^{81}\text{Br}) = 62.8(4)$ MHz and $C_Q(^{79}\text{Br}) = 75.1(5)$ MHz are by far the largest measured using $^{79/81}\text{Br}$ SSNMR spectroscopy.^{5,6} The nonaxial EFG ($\eta_Q = 0.445(20)$) underscores the low site symmetry, and restricts the rotational site symmetry to a maximum of C_2 , in agreement with the known site symmetry. A ν_Q measured using NQR spectroscopy may be related to C_Q when η_Q and I are also known:¹⁰⁶

$$\nu_Q = \frac{3C_Q\sqrt{1 + (\eta_Q^2/3)}}{2I(2I + 1)} \quad (1.2)$$

Using the measured ^{79}Br SSNMR parameters, $\nu_Q(^{79}\text{Br})$ is found to be 38.8 MHz, in perfect agreement with the NQR measurement. Quantitative agreement between NQR and NMR observations provides an experimental basis for our earlier assertion,⁵ based on exact theoretical modeling,¹⁰⁷ that substantial $C_Q(^{79/81}\text{Br})$ values may be accurately measured while remaining within the high-field approximation.

Using a series of M[BPh₄] salts (M = Na, K, Rb, Cs), Wu and Terskikh illustrated a linear relationship between measured $C_Q(M)$ values and $eQ(1 - \gamma_\infty)V$, where $(1 - \gamma_\infty)$ represents the Sternheimer antishielding and V is the unit cell volume.¹⁰⁸ In the present context, it is interesting to compare our $C_Q(^{81}\text{Br})$ for CaBr₂ with the $C_Q(^{35}\text{Cl})$ value measured for CaCl₂.⁵⁵ Using the parameters in Table S4 of the Supporting Information, it is

calculated that $|C_Q(^{81}\text{Br})/C_Q(^{35}\text{Cl})| = 7.12$. This is in severe disagreement with the value established from measurements, which is 29.9. Indeed, Stebbins et al. seemed rightfully surprised that the CaCl₂ structure, with its distorted trigonal planar geometry about the Cl and relatively short Cl–Ca distances, should possess a small $C_Q(^{35}\text{Cl})$. It is emphasized that CaBr₂ possesses the *largest* $C_Q(^{81}\text{Br})$ measured in our current study (vide infra). During their $^{35/37}\text{Cl}$ SSNMR study of alkaline earth metal chloride hydrates, Bryce and Bultz⁵⁶ noted that among the anhydrous compounds, the accepted $C_Q(^{35}\text{Cl})$ value⁵⁵ for CaCl₂ is the *smallest*, if one neglects the cubic SrCl₂ system. We are currently investigating this discrepancy.

Precise line-shape analysis (see Supporting Information, Figures S2 and S3, for select examples) allows for the first determination of bromine CSA in a powdered sample using multiple fields and multiple nuclide data sets, $\Omega = 250(150)$ ppm. Prior accounts of bromine CSA are limited to a single-crystal study on NaBrO₃ ($\Omega = 90$ ppm)¹⁰⁹ and a recent study of several powdered C_xH_{2x+1}(CH₃)_nBr systems.³² This recent account³² reported ⁸¹Br MAS SSNMR data at a single magnetic field and multiple MAS frequencies, followed by advanced line-shape fitting routines which incorporate QI/CSA interplay under MAS. The values of Ω were found to range from 23 ppm to 80 ppm; however, error bounds were not reported. Modest $C_Q(^{81}\text{Br})$ values (6.03 to 8.08 MHz), were also measured.

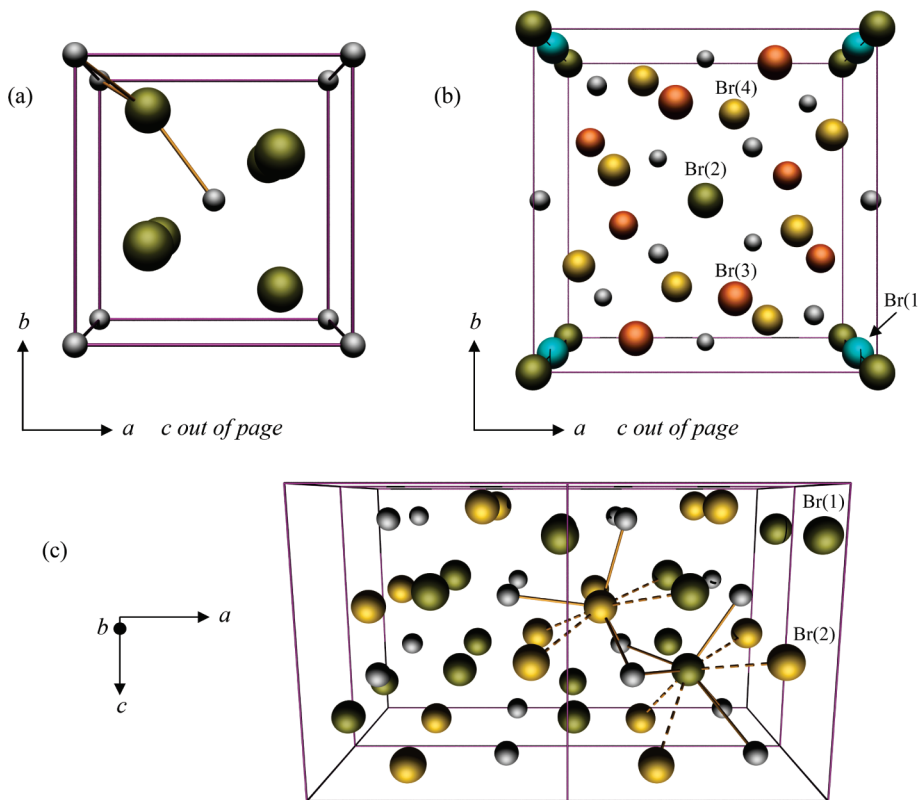


Figure 2. POV-ray renderings of various anhydrous alkaline earth metal bromides. For each, the metal cation is in gray. (a) CaBr_2 unit cell. Solid lines denote ions within the sum of the Ca and Br van der Waals (vdW) radii (i.e., $r < 4.14 \text{ \AA}$). All vdW radii are taken from refs 102 and 103. (b) SrBr_2 unit cell. The following color and labeling scheme is used to distinguish the four inequivalent Br: Br(1) = turquoise; Br(2) = green; Br(3) = orange; Br(4) = gold. (c) BaBr_2 quadruple unit cell, viewed nearly along b (rotated 10° counterclockwise about the positive a axis). The following color and labeling scheme is used: Br(1) = green; Br(2) = gold. Solid lines denote ions within the sum of the Ba and Br vdW radii (i.e., $r < 4.51 \text{ \AA}$), while dotted lines denote homoatomic contacts slightly beyond twice the Br vdW radius (i.e., slightly greater than 3.66 \AA).

The $^{79/81}\text{Br}$ SSNMR line shapes for CaBr_2 were relatively insensitive to κ , which is assumed to be near 0, as a result of GIPAW DFT computations (vide infra). The simulations shown in Figure 1e–h clearly demonstrate the presence of CSA and the noncoincidence of the \ddot{V} and $\ddot{\sigma}$ PASs. These findings are consistent with m site symmetry for the Br, which only restricts one principal axis of \ddot{V} and $\ddot{\sigma}$ to be collinear. The $^{79/81}\text{Br}$ NMR line-shape is also found to be sensitive to β , while α or γ variation leads to very subtle line-shape changes.

ii. SrBr_2 : A Test of the Resolving Power of $^{79/81}\text{Br}$ NMR. The static $^{79/81}\text{Br}$ SSNMR spectra of SrBr_2 are complex (see Figure 3) due to several overlapping signals. Accurate line-shape simulations were enabled by having four experimental data sets from which to draw. The parameters are reported in Table 1.

The ambient crystal structure of SrBr_2 ^{100,110,111} belongs to the tetragonal space group $P4/n$.¹¹² There are four crystallographic bromine sites in SrBr_2 . Two sites, labeled as Br(1) and Br(2), (Figure 2b) occupy $\bar{4}$ lattice sites, while the remaining two (Br(3) and Br(4)) are found at 1 lattice positions. Bromine-79 NQR data exist for two of the four sites (Table 1).¹⁰⁵ After a deconvolution of the $^{79/81}\text{Br}$ SSNMR line shapes (Figure 3g,j), it is clear that the two sites which possess η_Q near 0 and $\kappa = -1$ (indicative of axial $\ddot{\sigma}$ and \ddot{V}) are due to Br ions at $\bar{4}$ sites.¹¹³ With respect to one another, the Br ions at $\bar{4}$ sites possess very similar δ_{iso} (410(8) ppm and 422(5) ppm), although they are quite distinct from the third site ($\delta_{\text{iso}} = 320(10)$ ppm). As a result of GIPAW DFT computations (vide infra), the sites with $C_Q(^{81}\text{Br}) = 10.3(3)$ and $18.10(20)$ MHz are assigned to Br(1) and Br(2), respectively. The remaining signal (Br(3)) is assigned to a bromine at a 1 site in the lattice. The $\nu_Q(^{79}\text{Br})$ NQR values for SrBr_2 are too large to be assigned to either Br(1) or Br(2);

however, for Br(3), we have measured $C_Q(^{79}\text{Br}) = 30.6(2)$ MHz and $\eta_Q = 0.695(15)$. Using eq 1.2, this corresponds to $\nu_Q(^{79}\text{Br}) = 16.5$ MHz, in excellent agreement with the smaller of the two previously reported $\nu_Q(^{79}\text{Br})$ values (Table 1).

The three resolved sites have CSA, although each is more modest than in CaBr_2 . For Br(1) and Br(2), the rather small spans ($\Omega(\text{Br}(1)) = 50(20)$ ppm; $\Omega(\text{Br}(2)) = 85(25)$ ppm) are reflective of the small distortions from tetrahedral symmetry about these atoms. This is consistent with observations of small chlorine CSA for nearly tetrahedral chlorine environments, e.g., for dry $\text{LiAl}_2(\text{OH})_6\text{ClO}_4 \cdot n\text{H}_2\text{O}$, $\Omega = 32$ ppm.¹¹⁴ As Br(3) is at a 1 position, it is therefore expected that the measured Ω value would be larger, relative to Br(1) and Br(2). Indeed, this is in agreement with our observations ($\Omega(\text{Br}(3)) = 110(30)$ ppm). As with CaBr_2 , line-shape fits indicate noncoincident $\ddot{\sigma}$ and \ddot{V} PASs (see Supporting Information, Figure S4, for the models considered when fitting the $^{79/81}\text{Br}$ SSNMR line shapes of SrBr_2). Variation of β again produces significant change in simulated $^{79/81}\text{Br}$ SSNMR line shapes.

The ratio of the integrated intensities between the Br(1), Br(2), and Br(3) signals is $0.25 \pm 0.01:0.25 \pm 0.02:1$, in agreement with the accepted crystal structure; however, a fourth site is expected. Also, an additional signal, associated with a large ν_Q , was observed using ^{79}Br NQR. Hence, $^{79/81}\text{Br}$ SSNMR experiments were performed at $B_0 = 21.1$ T, this time scanning a greater frequency range. An additional site, (Br(4)), possessing a large ($C_Q(^{79}\text{Br}) = 64.2(6)$ MHz), nonaxial ($\eta_Q = 0.33(2)$) QI, is observed (Figure 4). The observed QI symmetry is consistent with a Br at a 1 lattice position. Using eq 1.2 and the above values of C_Q and η_Q , $\nu_Q(^{79}\text{Br}) = 32.7$ MHz for Br(4), in very

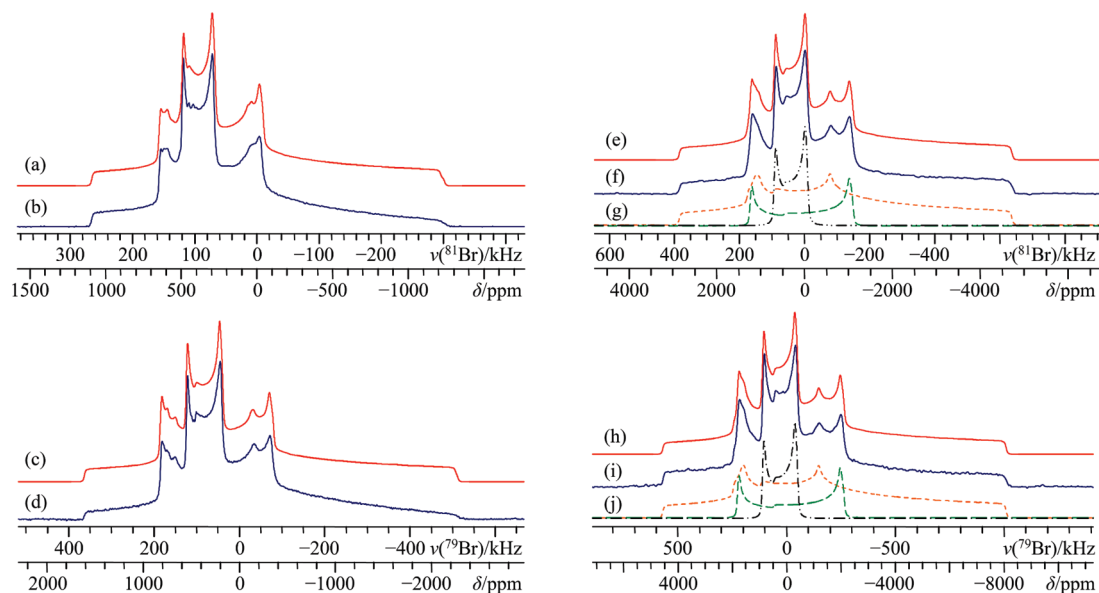


Figure 3. Analytical simulations (a, c), and experimental static VOCS Solomon echo (b, d) $^{79/81}\text{Br}$ SSNMR spectra of three of the four magnetically unique bromine sites in powdered SrBr_2 , acquired at $\mathbf{B}_0 = 21.1$ T. Analytical simulations (e, h), and experimental static VOCS Solomon echo (f, i) $^{79/81}\text{Br}$ SSNMR spectra of three of the four sites, acquired at $\mathbf{B}_0 = 11.75$ T. In g and j, a deconvolution of the three sites is provided.

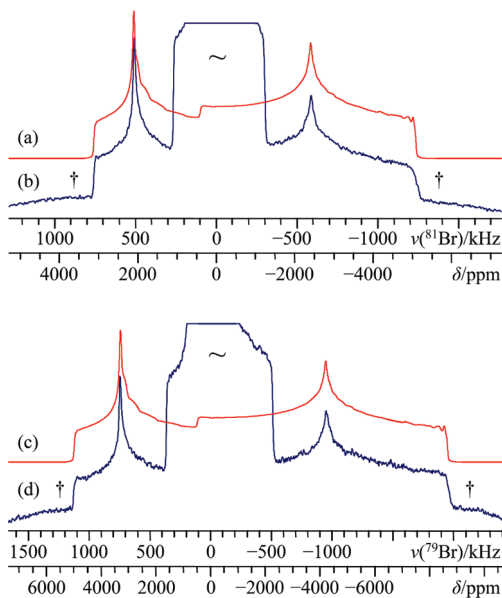


Figure 4. Analytical simulations (a, c), and experimental static VOCS Solomon echo (b, d) $^{79/81}\text{Br}$ SSNMR spectra of the broadest of the four SrBr_2 sites, acquired at $\mathbf{B}_0 = 21.1$ T. Partially excited ST are denoted using “†”. The spectral region corresponding to the three other SrBr_2 sites (partially cut off vertically) is denoted using “~”.

good agreement with the ^{79}Br NQR value. A reliable experimental estimate of the bromine CSA could not be obtained for this site.

Although four sites have been observed and grouped into Br belonging to 4 sites and those at 1 sites, it is difficult to assign them conclusively to individual crystallographic sites without considering additional information. Further discussion is postponed until we consider the results of GIPAW DFT computations.

iii. BaBr_2 : Deficiencies in ^{79}Br NQR Data. Static $^{79/81}\text{Br}$ SSNMR experiments on BaBr_2 at $\mathbf{B}_0 = 11.75$ T and $\mathbf{B}_0 = 21.1$ T yield well-defined spectra which exhibit many discontinuities (Figure 5). The two expected crystallographic sites are resolved (Figure 5b,d) and the $^{79/81}\text{Br}$ SSNMR parameters are precisely determined (Table 1).

Refined pXRD data have established that the stable orthorhombic form of BaBr_2 is isomorphic to BaCl_2 and crystallizes in the $Pnma$ space group.^{100,115} Both crystallographic bromines are at m sites, which requires one principal axis of \vec{V} to be collinear with one principal axis of $\vec{\sigma}$. A ^{79}Br NQR study measured two ν_Q values (in agreement with the proposed crystal structure) and highlighted the temperature-dependence of $\nu_Q(^{79}\text{Br})$.¹¹⁶ Bromine-79/81 SSNMR experiments have been carried out previously on this system,¹¹⁷ but the second-order line shapes were not resolved, the crystallographic sites were not distinguished, and discussion pertaining to $\vec{\sigma}$ and \vec{V} was not provided.

The measured $C_Q(^{79/81}\text{Br})$ values for the two bromine sites in BaBr_2 are quite similar. While the NMR observation of two sites agrees with all prior data, the ratio between the ^{79}Br C_Q s determined using NMR, and the ^{79}Br C_Q s (using eq 1.2) from NQR are in disagreement (Table 1). For example, for the Br(1) site in BaBr_2 (site label as a result of GIPAW DFT computations, vide infra), $C_Q(^{79}\text{Br}) = 28.1(4)$ MHz and $\eta_Q = 0.17(2)$; hence, $\nu_Q(\text{Br},\text{Br}(1)) = 14.1$ MHz, in good agreement with one of the ^{79}Br NQR signals. Using the same procedure for Br(2), $\nu_Q(^{79}\text{Br}) = 16.3$ MHz, in poor agreement with the NQR data. While the temperature variation in $\nu_Q(^{79}\text{Br})$ of Br(2), measured with NQR experiments, is significant (-20 kHz/K over the range $T = 77$ to 209 K), this alone cannot account for the discrepancies between the ^{79}Br SSNMR and NQR data. It is believed that the NQR datum is in error, as GIPAW calculations (vide infra) do not support substantially different QIs at the two Br sites in BaBr_2 , in agreement with our experimental results. After extensive searching for an additional broad ^{81}Br SSNMR signal at both 11.75 and 21.1 T, it was concluded that only two magnetically unique Br sites were present. According to the authors of the NQR study in ref 116, the “signal-to-noise ratio with maximum sensitivity of the instrument did not exceed 1.5–2”. Hence, it is entirely possible that the two sites were not resolved via ^{79}Br NQR, and that the high ν_Q signal was due to an impurity.

A ^{35}Cl SSNMR study on the isomorphic BaCl_2 resolved two sites with similar $C_Q(^{35}\text{Cl})$ values.¹¹⁸ If we consider the $|C_Q(^{81}\text{Br})|$

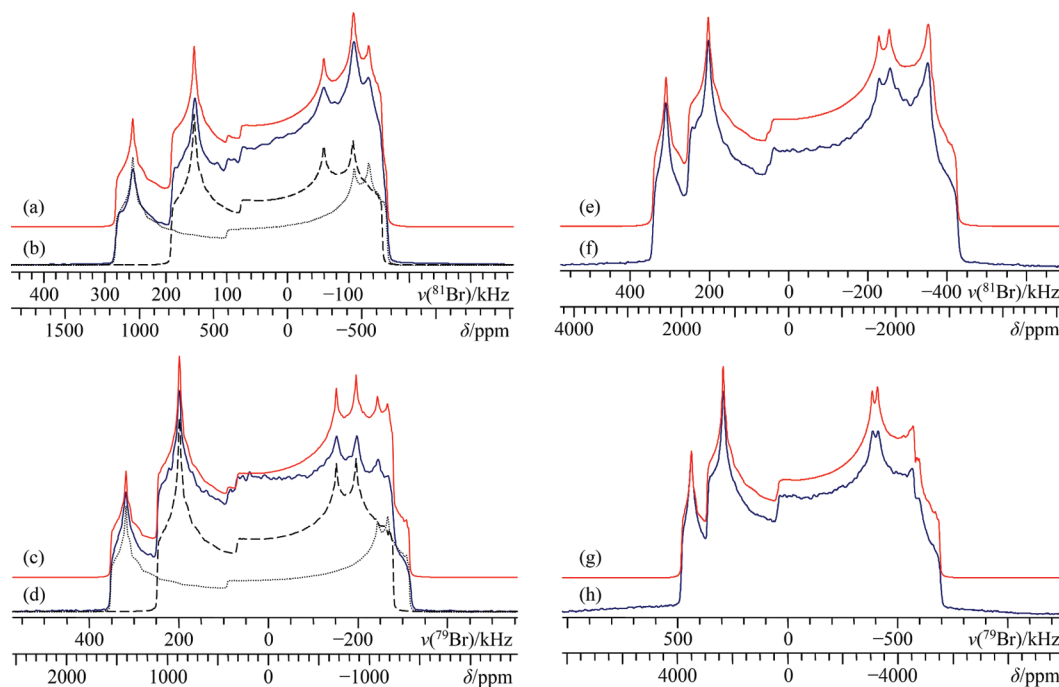


Figure 5. Analytical simulations (a, c, e, g), experimental static Solomon echo (b), and experimental static VOCS Solomon echo (d, f, h) $^{79/81}\text{Br}$ SSNMR spectra of powdered BaBr_2 , acquired at $\mathbf{B}_0 = 21.1$ T (b, d) and 11.75 T (f, h). A deconvolution of the two sites is provided in b and d (dashed and dotted traces).

TABLE 2: Experimental $^{79/81}\text{Br}$ EFG and Chemical Shift Tensor Parameters: Alkaline Earth Metal Bromide Hydrates^a

compound	site label	$ C_Q(^{81}\text{Br}) /\text{MHz}$	$ C_Q(^{79}\text{Br}) /\text{MHz}$	η_Q	$\delta_{\text{iso}}/\text{ppm}$	Ω/ppm	κ	α/deg	β/deg	γ/deg	$\nu_Q(^{79}\text{Br})/\text{MHz}^b$
$\text{MgBr}_2 \cdot 6\text{H}_2\text{O}$	—	19.0(2)	22.7(2)	0.23(3)	57(7)	50(20)	0.7(0.3)	170(10)	57(10)	180 ^c	—
$\text{SrBr}_2 \cdot 6\text{H}_2\text{O}$	—	27.7(3)	33.2(3)	<0.01	95(15)	70(30)	-1 ^d	210 ^c	90(20)	180(10)	—
$\text{BaBr}_2 \cdot 2\text{H}_2\text{O}$	—	7.32(3)	8.74(4)	0.76(2)	218.2(1.0)	86(5)	-0.20(0.15)	70(5)	95(8)	253(5)	4.58(0.05)
$\text{CaBr}_2 \cdot x\text{H}_2\text{O}$	Br(1)	—	—	—	-55(4)	—	—	—	—	—	—
	Br(2)	12.8(4)	15.4(5)	0.32(4)	205(15)	—	—	—	—	—	—
	Br(3)	23.0(4)	27.6(5)	0.25(3)	170(15)	—	—	—	—	—	—

^a Error bounds are in parentheses. Parameter definitions are in the main text. ^b From literature, ref 116. The measurement occurred at $T = 209$ K. ^c Simulated NMR line-shape is insensitive to parameter variation. The value is assigned based on computational results. ^d Assumed based on crystallographic site symmetry.

$C_Q(^{35}\text{Cl})$ value for both sites using the approach outlined earlier for CaBr_2 , it is calculated (see Supporting Information, Table S4, for parameters used) as 7.09 for both sites. Experimentally, $|C_Q(^{81}\text{Br})/C_Q(^{35}\text{Cl})| = 6.71$ and 6.89 for sites 1 and 2, respectively, which is in good agreement, especially when noting that chlorine CSA was not considered in the ^{35}Cl SSNMR fits.¹¹⁸ For both BaCl_2 and BaBr_2 , the site with the larger halogen C_Q is associated with a much greater δ_{iso} . Likewise, when comparing measured halogen η_Q values, it is observed that within experimental error, Br(1) agrees with “Cl(1)” and Br(2) agrees with “Cl(2)”, as expected by symmetry.

B. Stable Hydrates of the Alkaline Earth Metal Bromides. Using a series of alkaline earth metal chloride hydrates, it has been shown that $^{35/37}\text{Cl}$ SSNMR spectroscopy is sensitive to pseudopolymorphism.⁵⁶ Presently, the results of $^{79/81}\text{Br}$ SSNMR experiments at multiple applied fields on $\text{BaBr}_2 \cdot 2\text{H}_2\text{O}$, $\text{MgBr}_2 \cdot 6\text{H}_2\text{O}$, and $\text{SrBr}_2 \cdot 6\text{H}_2\text{O}$, are discussed. The data are summarized in Table 2.

i. $\text{BaBr}_2 \cdot 2\text{H}_2\text{O}$: An Example of ^{79}Br MAS NMR. Static $^{79/81}\text{Br}\{^1\text{H}\}$ SSNMR experiments at $\mathbf{B}_0 = 11.75$ and 21.1 T reveal relatively narrow (~ 100 kHz) bromine NMR line shapes (Figure 6). The relatively small QI ($C_Q(^{81}\text{Br}) = 7.32(3)$ MHz) allows for MAS NMR experiments to be performed at $\mathbf{B}_0 = 21.1$ T (Figure 7), which represents the first report of ^{79}Br MAS SSNMR of a spectrum broadened by a second-order QI. As

the CT centerband under MAS conditions depends only upon δ_{iso} , C_Q , and η_Q , the measurement errors associated with the $^{79/81}\text{Br}$ SSNMR parameters are greatly reduced relative to the anhydrous samples.

Single-crystal XRD^{119,120} and neutron diffraction¹²¹ studies confirm that $\text{BaBr}_2 \cdot 2\text{H}_2\text{O}$ belongs to the monoclinic $C2/c$ space group. The bromine atoms are at 1 lattice positions, which place no symmetry restrictions on the QI and CSA tensor parameters. Single crystal ^1H NMR studies on this system have focused on the location and dynamics of the H atoms,^{122–126} and IR spectroscopy has been used to establish the presence of H_2O librational motions at room temperature.¹²⁷

The difference in QI magnitude between the hydrated and anhydrous pseudopolymorphs shows that $^{79/81}\text{Br}$ SSNMR spectroscopy is a very sensitive method to determine the hydration state of BaBr_2 . Spectral acquisition is rapid: a high quality static $^{81}\text{Br}\{^1\text{H}\}$ SSNMR spectrum of the hydrate can be obtained in under 15 min at 11.75 T. The bromine $\ddot{\nu}$ and $\ddot{\sigma}$ tensors in the dihydrate are nonaxial ($\eta_Q = 0.76(2)$; $\kappa = -0.20(0.15)$) and their PAss are noncoincident. As shown in Figure 6c, due to (i) the proximity of the ^1H and $^{79/81}\text{Br}$ nuclei and (ii) the relatively narrow signal, ^1H decoupling is essential to observe the fine structure in these $^{79/81}\text{Br}$ SSNMR line shapes. A ^{79}Br NQR study at 209 K measured $\nu_Q(^{79}\text{Br}) = 4.58(0.05)$ MHz.¹¹⁶ Using our $C_Q(^{79}\text{Br})$ and η_Q values and applying eq 1.2, we find

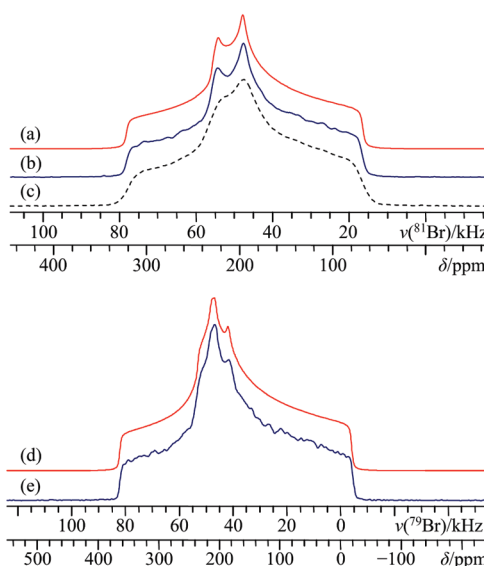


Figure 6. Analytical simulations (a, d, f, h) and experimental static Solomon echo (b, c, e, g, i) $^{79/81}\text{Br}\{{}^1\text{H}\}$ SSNMR spectra of powdered $\text{BaBr}_2 \cdot 2\text{H}_2\text{O}$, acquired at $\mathbf{B}_0 = 21.1$ T (b, c, e) and 11.75 T (g, i). In c, ${}^1\text{H}$ decoupling is not applied.

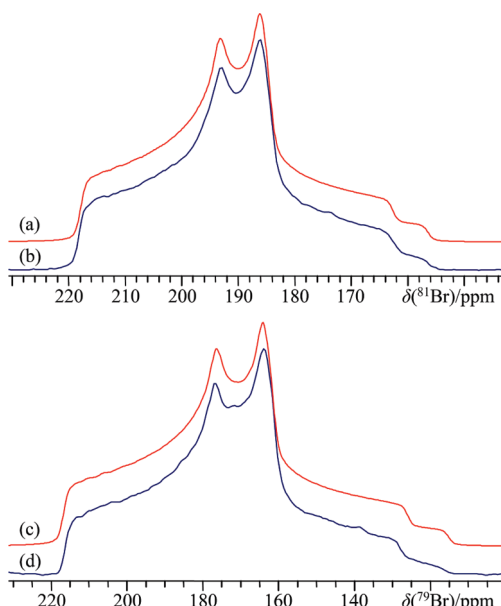


Figure 7. Analytical simulations (a, c), and experimental MAS Solomon echo (b, d) $^{79/81}\text{Br}\{{}^1\text{H}\}$ SSNMR spectra of powdered $\text{BaBr}_2 \cdot 2\text{H}_2\text{O}$, acquired at $\mathbf{B}_0 = 21.1$ T with (b) $v_{\text{rot}} = 20.000$ kHz; (d) $v_{\text{rot}} = 26.318$ kHz.

that $\nu_Q(\text{Br}) = 4.77$ MHz, which is in fair agreement with the NQR finding, especially when noting that the librational motion of the water molecules is not equivalent at both temperatures.

In addition to the significant change in the QI at the Br nuclei, the bromine chemical shift of $\text{BaBr}_2 \cdot 2\text{H}_2\text{O}$ is reduced relative to either Br site in BaBr_2 . In fact, it is more shielded than any anhydrous bromide site by at least 60 ppm. This decrease in chemical shift upon hydration is consistent with the trend observed in the $^{35/37}\text{Cl}$ SSNMR spectra of the analogous alkaline earth metal chloride systems.^{55,56,118} The decreased shift upon hydration is corroborated by GIPAW DFT computations (vide infra). Hence, it appears that the bromine δ_{iso} is also a reliable indicator of the presence of hydration for alkaline earth metal bromide systems.

ii. $\text{MgBr}_2 \cdot 6\text{H}_2\text{O}$ and $\text{SrBr}_2 \cdot 6\text{H}_2\text{O}$: On the Relationship between Bromine NMR Parameters and Hydration State. Static $^{79/81}\text{Br}$ SSNMR spectra for both these compounds were collected

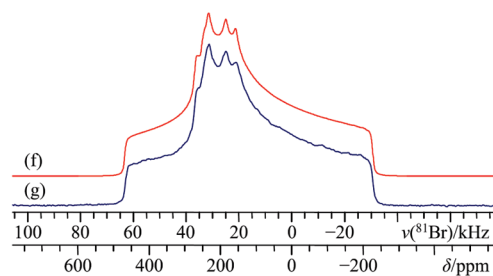


Figure 8. Analytical simulations (a, d, f), experimental static Solomon echo (b, c, e), and experimental static VOCS Solomon echo (g) $^{79/81}\text{Br}\{{}^1\text{H}\}$ SSNMR spectra of powdered $\text{MgBr}_2 \cdot 6\text{H}_2\text{O}$, acquired at $\mathbf{B}_0 = 21.1$ T (b, c) and 11.75 T (e, g). Low power ${}^1\text{H}$ decoupling ($\nu_{\text{rf}}({}^1\text{H}) \approx 40$ kHz) is applied to acquire e and g and does not lead to significant line-shape distortions, while high power ${}^1\text{H}$ decoupling ($\nu_{\text{rf}}({}^1\text{H}) \approx 100$ kHz) causes probe heating, leading to a detectable alteration in the QI at the Br nuclei in c.

at $\mathbf{B}_0 = 11.75$ and 21.1 T. The spectra exhibit similar line-shape features as the systems discussed above (Figures 8, 9; and Supporting Information, Figure S5) and were precisely fit (Table 2).

The space group ($C2/m$), unit cell parameters, and atomic positions of $\text{MgBr}_2 \cdot 6\text{H}_2\text{O}$ were initially reported in 1934,^{92,128} and a precise determination of the unit cell was later carried out.⁹³ There is one unique bromine crystallographic site, which

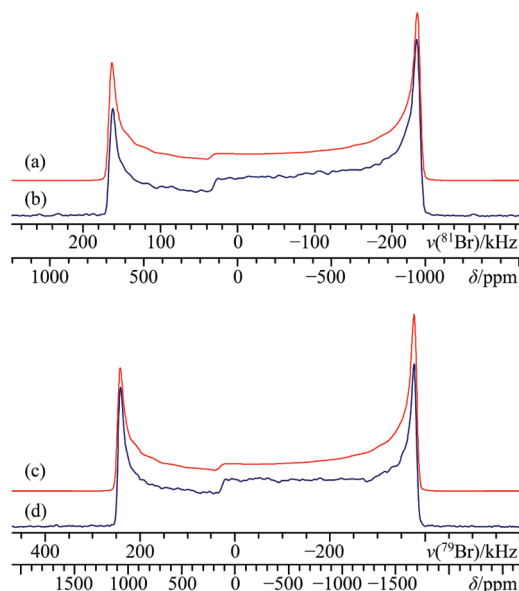


Figure 9. Analytical simulations (a, c), experimental static Solomon echo (b), and experimental static VOCS Solomon echo (d) $^{79/81}\text{Br}$ SSNMR spectra of powdered $\text{SrBr}_2 \cdot 6\text{H}_2\text{O}$, acquired at $\mathbf{B}_0 = 21.1$ T. High power ^1H decoupling ($\nu_{\text{rf}}(^1\text{H}) \approx 100$ kHz) did not alter the $^{79/81}\text{Br}$ SSNMR signal significantly (i.e., within our measurement errors).

possesses m symmetry. Neutron diffraction data do not exist for this compound; hence, the H positions are unknown. However, they should be very similar to the H positions in the isomorphic compound $\text{MgCl}_2 \cdot 6\text{H}_2\text{O}$, whose structure was determined using neutron diffraction.¹²⁹ There are no prior $^{79/81}\text{Br}$ NQR data for $\text{MgBr}_2 \cdot 6\text{H}_2\text{O}$, although ^{25}Mg NQR¹³⁰ and ^1H SSNMR¹³¹ measurements have been reported. These previous studies highlighted a small ^{25}Mg QI, and the isotropic motion of the H_2O molecules at room temperature, respectively.

As with $\text{BaBr}_2 \cdot 2\text{H}_2\text{O}$, $\text{MgBr}_2 \cdot 6\text{H}_2\text{O}$ has a relatively small, nonaxial QI ($C_Q(^{81}\text{Br}) = 19.0(2)$ MHz; $\eta_Q = 0.23(3)$) and is significantly more shielded ($\delta_{\text{iso}} = 57(7)$ ppm) than its anhydrous pseudopolymorph.⁴ The observed bromine NMR line shapes, especially the ^{81}Br SSNMR signal acquired at 21.1 T, clearly exhibit nonaxial and noncoincident $\dot{\nu}$ and $\ddot{\sigma}$ tensors (Figure 8). The feature in the low frequency portion of Figure 8b,c,e indicates that β is not equal to 0° or 90° ($\beta = 57(10)^\circ$). All findings are consistent with the known Br crystal site symmetry and are in fair agreement with GIPAW DFT calculations (vide infra). Finally, the calculated ratio $|C_Q(^{81}\text{Br})/C_Q(^{35}\text{Cl})|$ for the $\text{MgBr}_2 \cdot 6\text{H}_2\text{O}$ and $\text{MgCl}_2 \cdot 6\text{H}_2\text{O}$ isomorphs is found to be 6.73 (see Supporting Information, Table S4, for parameters used), in reasonable agreement with the experimentally observed ratio of 6.29.⁵⁶

The crystal structure of $\text{SrBr}_2 \cdot 6\text{H}_2\text{O}$ has been solved using XRD^{94,132} and belongs to the same space group ($P321$) as $\text{SrCl}_2 \cdot 6\text{H}_2\text{O}$, $\text{CaCl}_2 \cdot 6\text{H}_2\text{O}$, and $\text{CaBr}_2 \cdot 6\text{H}_2\text{O}$.^{95,96} In these systems, there is one magnetically unique halogen, located on a C_3 axis. Br-79/81 NQR data are not available for $\text{SrBr}_2 \cdot 6\text{H}_2\text{O}$. According to ^1H SSNMR findings, the H_2O molecules in the strontium hydrate are stationary at room temperature.¹³³ The static Solomon echo $^{79/81}\text{Br}$ SSNMR spectra at 11.75 and 21.1 T are fit using axially symmetric (i.e., $\eta_Q < 0.01$; $\kappa = -1.0$) EFG and CSA parameters (Figure 9 and Supporting Information, Figure S5). Axially symmetric tensors are expected according to the accepted crystal structure. Relative to the magnesium hydrate, the QI is larger ($C_Q(^{81}\text{Br}) = 27.7(3)$ MHz), but once again for a hydrate, δ_{iso} is much lower than for the corresponding

anhydrous compound ($\delta_{\text{iso}} = 95(15)$ ppm). The CSA in this compound is relatively small ($\Omega = 70(30)$), and the simulated line-shape is particularly sensitive to the β value. The ratio $|C_Q(^{81}\text{Br})/C_Q(^{35}\text{Cl})|$ for the $\text{SrCl}_2 \cdot 6\text{H}_2\text{O}$ and $\text{SrBr}_2 \cdot 6\text{H}_2\text{O}$ isomorphs was calculated to be 6.55 (using the parameters in the Supporting Information, Table S4), in fair agreement with the experimentally observed ratio of 7.08.⁵⁶

C. $\text{CaBr}_2 \cdot x\text{H}_2\text{O}$: Characterization of a Mixture of Unknown Composition. Calcium bromide is hygroscopic and hence is commercially available as a “hydrate” mixture of unknown composition, $\text{CaBr}_2 \cdot x\text{H}_2\text{O}$, where $x \approx 1$. A VOCS Solomon echo ^{81}Br SSNMR spectrum of the mixture, acquired at $\mathbf{B}_0 = 21.1$ T (Figure 10h), resolves four components. The broadest signal is fit to ^{81}Br SSNMR parameters characteristic of CaBr_2 (e.g., $C_Q(^{81}\text{Br}) = 62.7(5)$ MHz). A VOCS QCPMG ^{81}Br SSNMR experiment performed on this mixture at $\mathbf{B}_0 = 11.75$ T also resolves the broad signal (see Supporting Information, Figure S6). The remaining three sites are observed in Solomon echo ^{81}Br SSNMR spectra acquired at 21.1 and 11.75 T (Figure 10b,e), as well as ^{79}Br SSNMR spectra acquired at both fields (see Supporting Information, Figure S7). The three narrow signals were deconvoluted and fit using the parameters in Table 2.

Due to its bromine chemical shift, and lack of significant QI or CSA, site 1 is assigned to NaBr .⁵ This assignment is further supported by the observation of a narrow ^{23}Na signal, which was serendipitously measured while acquiring the QCPMG ^{81}Br SSNMR spectrum of the mixture at 11.75 T (Supporting Information, Figure S6). The remaining two sites are due to CaBr_2 hydrates. By observing the δ_{iso} values, it is suspected that the hexahydrate pseudopolymorph⁹⁶ is not present. This is due to our observations above, where δ_{iso} for the hexahydrates are below 100 ppm. Likewise, GIPAW DFT computations using the known $\text{CaBr}_2 \cdot 6\text{H}_2\text{O}$ crystal structure⁹⁶ predict an axial QI and low chemical shift (Table 4), both in disagreement with experiment. Hence, the presence of $\text{CaBr}_2 \cdot 6\text{H}_2\text{O}$ is very unlikely.

In addition to the hexahydrate, a detailed study by Paulik et al. established the existence of mono-, di-, and tetrahydrates of CaBr_2 .¹³⁴ To the best of our knowledge, the crystal structures for these hydrates are not known. Using ^{79}Br NQR, Smirnov and Volkov reported that $\nu_Q(^{79}\text{Br}) = 19.09$ MHz at $T = 300$ K for $\text{CaBr}_2 \cdot \text{H}_2\text{O}$.¹⁰⁵ Using our ^{79}Br SSNMR parameters and eq 1.2, $\nu_Q(^{79}\text{Br}) = 7.88$ and 14.1 MHz for sites 2 and 3, respectively. Both are in significant disagreement with the accepted value for $\text{CaBr}_2 \cdot \text{H}_2\text{O}$, and hence the presence of the monohydrate is unlikely. The remaining known hydrates of CaBr_2 , namely $\text{CaBr}_2 \cdot 2\text{H}_2\text{O}$ and $\text{CaBr}_2 \cdot 4\text{H}_2\text{O}$, are likely the remaining components in the mixture.

Integrated intensity measurements of the $^{79/81}\text{Br}$ SSNMR signals at two fields establish that $61 \pm 2\%$ of the bromine signal intensity is due to CaBr_2 , $24 \pm 2\%$ is due to site 2 and $15 \pm 2\%$ is due to site 3. Incidentally, the integrated intensity of the NaBr signal is $<1\%$, hinting that $^{79/81}\text{Br}$ SSNMR experiments are a sensitive method for the detection of cubic bromide impurities. If site 2 is assigned to the dihydrate and site 3 to the tetrahydrate, then $x \approx 1.08$, which is in fair agreement with the value listed by the manufacturer. If the opposite assignment is made, then $x \approx 1.26$, in poor relative agreement. Similarly, it has been established in the above sections, and for the corresponding chlorides,⁵⁶ that a negative correlation exists between $\delta_{\text{iso}}(\text{Br})$ and the degree of hydration (i.e., a decreased δ_{iso} is observed with increased hydration). Thus, the assignment

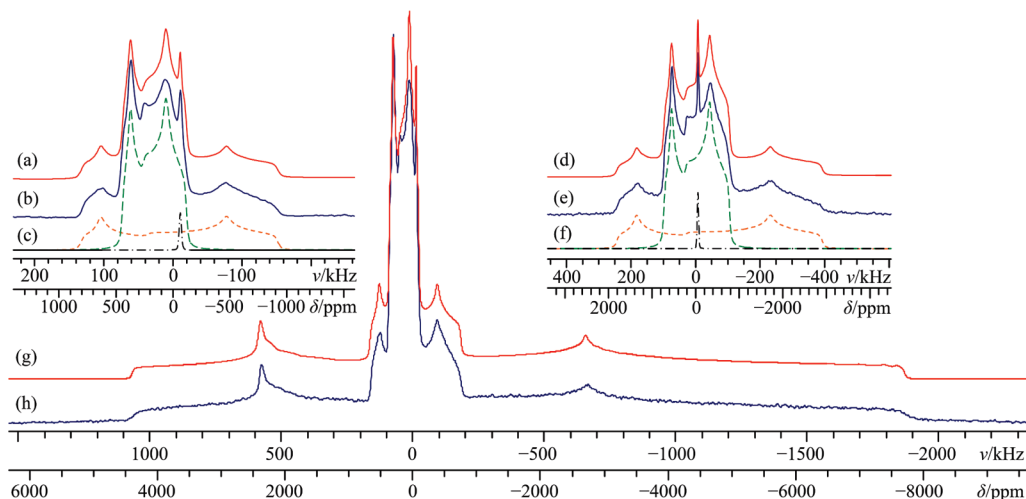


Figure 10. Analytical simulations (a, g), and experimental static VOCS Solomon echo (b, h) ^{81}Br SSNMR spectra of powdered $\text{CaBr}_2 \cdot x\text{H}_2\text{O}$, acquired at $\mathbf{B}_0 = 21.1$ T. Analytical simulation (d) and experimental (e) ^{81}Br SSNMR spectrum of the three central signals, acquired at $\mathbf{B}_0 = 11.75$ T. In c and f, a deconvolution of the central three sites is provided.

TABLE 3: GIPAW DFT-Computed ^{81}Br EFG and Chemical Shift Tensor Parameters: Anhydrous Alkaline Earth Metal Bromides^a

compound	functional	site label	$C_Q(^{81}\text{Br})/\text{MHz}^b$	η_Q	Ω/ppm	κ	$\delta_{\text{iso}}/\text{ppm}$	α/deg	β/deg	γ/deg
CaBr_2	PBE	—	-69.15	0.496	351.1	0.06	390.4	270.0	89.5	180.0
	PW91	—	-69.53	0.498	354.1	0.07	398.4	270.0	89.5	180.0
SrBr ₂	PBE	Br(1)	-9.80	0.000	57.96	-1.00	487.3	90.0	90.0	180.0
	Br(2)	-17.72	0.000	110.2	-1.00	462.7	90.0	90.0	180.0	
	Br(3)	-27.16	0.827	132.6	0.11	366.4	43.3	88.4	231.9	
	Br(4)	-60.43	0.297	182.5	-0.19	352.4	242.4	72.5	214.5	
	PW91	Br(1)	-9.83	0.000	56.7	-1.00	486.0	90.0	90.0	180.0
	Br(2)	-17.82	0.000	107.5	-1.00	460.7	90.0	90.0	180.0	
	Br(3)	-27.22	0.837	128.8	0.13	364.2	44.3	88.3	233.3	
	Br(4)	-60.86	0.298	181.0	-0.18	349.1	242.4	72.5	213.8	
BaBr ₂	PBE	Br(1)	-20.49	0.093	252.3	-0.48	333.3	0.0	49.6	180.0
	Br(2)	31.52	0.082	208.3	0.18	532.8	180.0	19.2	180.0	
	PW91	Br(1)	-20.60	0.098	253.0	-0.47	336.3	0.0	49.6	180.0
	Br(2)	31.71	0.082	209.3	0.19	537.4	180.0	19.4	180.0	

^a Parameter definitions are in the main text. CaBr_2 calculations used $E_{\text{cut}} = 800$ eV and a $5 \times 5 \times 8$ k-point grid; SrBr_2 calculations used $E_{\text{cut}} = 500$ eV and a $3 \times 3 \times 5$ k-point grid; BaBr_2 calculations used $E_{\text{cut}} = 600$ eV and a $3 \times 5 \times 3$ k-point grid. For further details, see Supporting Information: Tables S2, S3, and S5. ^b To convert $V_{33}(^{81}\text{Br})$ into frequency units, a conversion factor of 61.56077 MHz/a.u. was used, and the unit EFG is $9.71736166 \times 10^{21} \text{ J C}^{-1} \text{ m}^{-2}$.

TABLE 4: GIPAW DFT-Computed ^{81}Br EFG and Chemical Shift Tensor Parameters: Alkaline Earth Metal Bromide Hydrates^a

compound	functional	model label	$C_Q(^{81}\text{Br})/\text{MHz}$	η_Q	Ω/ppm	κ	$\delta_{\text{iso}}/\text{ppm}$	α/deg	β/deg	γ/deg
$\text{MgBr}_2 \cdot 6\text{H}_2\text{O}$	PBE	A	26.37	0.014	59.4	0.46	3.0	0.0	58.1	0.0
	PW91	A	26.02	0.018	60.2	0.44	3.7	0.0	57.9	0.0
	PBE	B	25.68	0.137	64.0	0.31	8.6	270.0	55.2	180.0
	PW91	B	25.34	0.133	64.8	0.29	9.4	270.0	55.1	180.0
$\text{CaBr}_2 \cdot 6\text{H}_2\text{O}$	PBE	—	-34.44	0.000	41.0	-1.00	62.1	247.2	89.8	180.2
	PW91	—	-34.38	0.000	40.8	-1.00	62.0	223.1	89.9	180.3
$\text{SrBr}_2 \cdot 6\text{H}_2\text{O}$	PBE	A	-18.42	0.000	31.5	-1.00	68.2	224.3	89.9	180.4
	PW91	A	-18.39	0.000	31.2	-1.00	67.2	226.6	89.9	180.4
	PBE	B	-40.97	0.000	80.7	-1.00	41.1	210.9	90.0	180.2
	PW91	B	-41.01	0.000	80.6	-1.00	40.3	212.2	90.0	180.2
$\text{BaBr}_2 \cdot 2\text{H}_2\text{O}$	PBE	—	-8.73	0.395	94.1	-0.24	199.5	61.0	84.1	240.7
	PW91	—	-9.09	0.411	94.4	-0.23	202.5	64.0	84.5	240.6

^a $\text{MgBr}_2 \cdot 6\text{H}_2\text{O}$ calculations used $E_{\text{cut}} = 750$ eV and a $2 \times 3 \times 4$ k-point grid; $\text{CaBr}_2 \cdot 6\text{H}_2\text{O}$ calculations used $E_{\text{cut}} = 610$ eV and a $4 \times 4 \times 6$ k-point grid; $\text{SrBr}_2 \cdot 6\text{H}_2\text{O}$ calculations used $E_{\text{cut}} = 800$ eV and a $4 \times 4 \times 6$ k-point grid; $\text{BaBr}_2 \cdot 2\text{H}_2\text{O}$ calculations used $E_{\text{cut}} = 800$ eV and a $3 \times 3 \times 3$ k-point grid. See also footnote b of Table 3. For further details, see Supporting Information: Tables S2, S3, and S6.

of $\text{CaBr}_2 \cdot 2\text{H}_2\text{O}$ to the site with a greater δ_{iso} is consistent with this correlation.

2. GIPAW Quantum Chemical Computations. To complement the experimental $^{79/81}\text{Br}$ SSNMR observations, all pure systems were subjected to GIPAW DFT quantum chemical calculations, the results of which are presented in Tables 3 and

4. Norm-conserving¹³⁵ and “ultrasoft” pseudopotential^{81,136} GI-PAW DFT methods⁸⁰ have been used to calculate δ tensors in a variety of systems for several NMR-active nuclei.^{82,137–140} For the calculation of \ddot{V} , modified PAW DFT methods^{141,142} have been applied to oxygen-containing systems.^{82,143,144} Recent studies employing the GIPAW DFT method include aluminum-

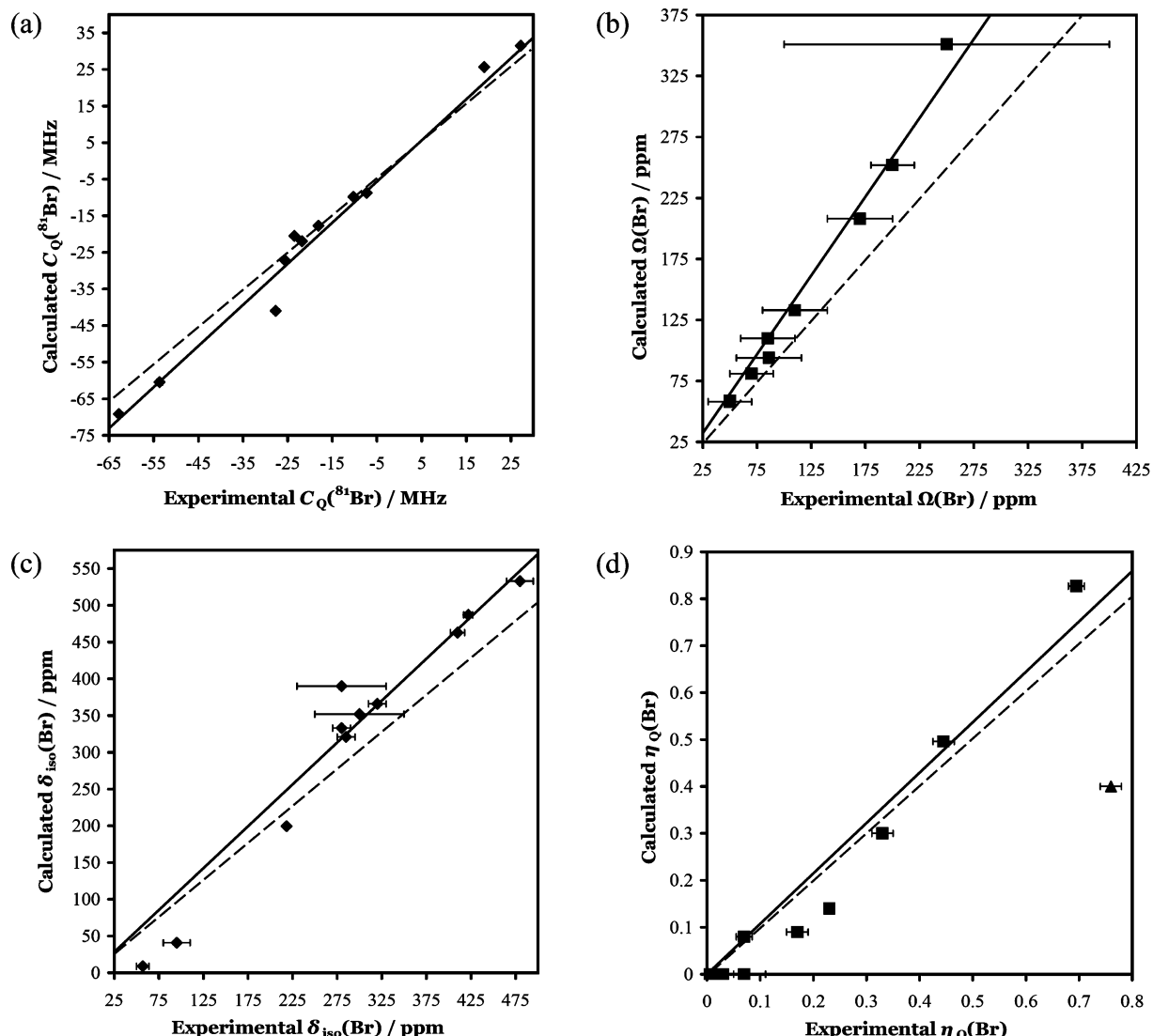


Figure 11. Plot of (a) GIPAW DFT-calculated versus experimental values for $C_Q(^{81}\text{Br})$, (b) for Ω , (c) for δ_{iso} , and (d) for η_Q . Experimental data are from Tables 1 and 2, while calculated data are from Tables 3 and 4. All values are from PBE XC functional calculations. Values for MgBr₂ are included, from ref 4. For MgBr₂·6H₂O and SrBr₂·6H₂O, the model B computed values are used. Solid lines are of best linear fit, while dashed lines denote an ideal fit (i.e., $y = x$): $C_Q(^{81}\text{Br}, \text{calc}) = 1.1235(C_Q(^{81}\text{Br}, \text{expt}))$, $R^2 = 0.982$, rmsd = 5.55 MHz; $\Omega(\text{calc}) = 1.2921(\Omega(\text{expt}))$, $R^2 = 0.981$, rmsd = 42.2 ppm; $\delta_{\text{iso}}(\text{calc}) = 1.1395(\delta_{\text{iso}}(\text{expt}))$, $R^2 = 0.946$, rmsd = 57.7 ppm; $\eta_Q(\text{calc}) = 1.0737(\eta_Q(\text{expt}))$, $R^2 = 0.946$, rmsd = 0.0649. In d, the line of best fit and rmsd omits the data point for BaBr₂·2H₂O (\blacktriangle).

containing oxides,¹⁴⁵ inorganic calcium materials,^{146,147} alkaline earth metal chlorides,⁵⁶ and amino acids.⁵¹ The first reported GIPAW DFT calculations of ^{79/81}Br NMR parameters were used by us as part of the structural refinement of MgBr₂.⁴ This account demonstrated that the $\ddot{\mathcal{V}}$ tensor at the bromine could be accurately calculated in MgBr₂, and that the bromine EFG was extremely sensitive to structure.

A. Calculated Bromine $\ddot{\mathcal{V}}$ and $\ddot{\sigma}$ Tensor Magnitudes and Symmetries. Agreement between experimental and GIPAW DFT-computed ^{79/81}Br NMR parameters is very good for several parameters (Figure 11). Relative to the experimental values, computed $C_Q(^{81}\text{Br})$ values are slightly higher in most cases, while the computed Ω values are higher in all cases. Only the computed and experimental Ω values for BaBr₂ are in disagreement with one another, after considering the errors associated with the measurement of Ω . The consistent overestimation of computed span values suggests the possibility of nonnegligible relativistic contributions to bromine shielding, as is generally observed in diatomic systems.¹⁴⁸ Rather good agreement is also seen between experimental and computed δ_{iso} and η_Q values.

With respect to the experimental values of δ_{iso} , all computed data for the anhydrous compounds are overestimated, while all computed values for the hydrates are underestimated. For all compounds except BaBr₂·2H₂O, agreement between the calculated and experimental η_Q values is very good. Where experimental Euler angles were measured, agreement between computation and experiment is excellent. The slightly increased discrepancy between experimental and computed NMR parameters for BaBr₂·2H₂O could be due to the librational motions of the H₂O molecules.¹²⁷ Only the α value computed for MgBr₂·6H₂O cannot be reconciled with experiment, although the XRD data used to solve for the structure of this compound carried large measurement errors.⁹² An additional structural model can be proposed that remains within the XRD measurement errors, while resulting in somewhat better agreement between the computed and experimental NMR parameters, most notably the clearly nonzero experimental value for η_Q (Table 4).

The reported structure for SrBr₂·6H₂O⁹⁴ should be isomorphic to SrCl₂·6H₂O; however, the reported structure places Br atoms

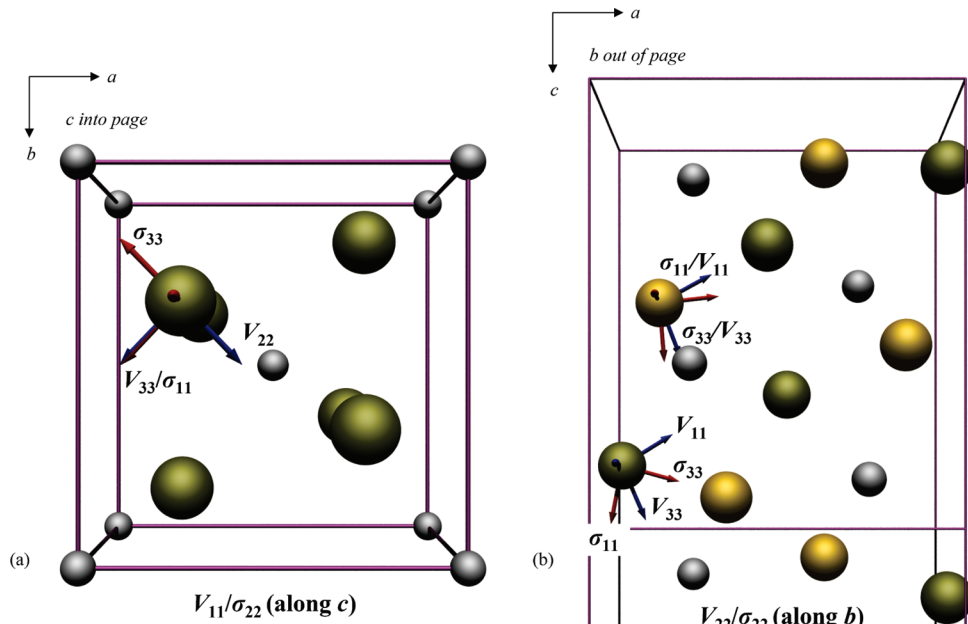


Figure 12. POV-Ray renderings of computed bromine \ddot{V} (V_{ii} , $i = 1, 2, 3$, in blue) and symmetric $\ddot{\sigma}$ (σ_{ii} , red) tensor eigenvectors in the crystal frame of (a) CaBr_2 and (b) BaBr_2 . For each, the metal cation is in gray, and the orientation is such that the mirror plane lies parallel to the page. CaBr_2 : $E_{\text{cut}} = 800$ eV, and a $5 \times 5 \times 8$ k-point grid; BaBr_2 : $E_{\text{cut}} = 600$ eV, and a $3 \times 5 \times 3$ k-point grid. Both employed the PBE XC functional. For b, the unique bromine sites are Br(1) (green) and Br(2) (gold). Eigenvectors are displayed once per unique Br and were placed using Diamond 3.2.

at $(a, b, -c)$, while (a, b, c) would place them in positions isomorphic to $\text{SrCl}_2 \cdot 6\text{H}_2\text{O}$ (see the Experimental Section for details). Hence, computations using both sets of Br atomic values, optimizing the H positions for each prior to NMR parameter computations, were carried out. Although inconclusive, NMR parameter agreement is slightly better for the model which places the Br atoms in positions isomorphic to $\text{SrCl}_2 \cdot 6\text{H}_2\text{O}$ (i.e., model B). This is primarily due to the drastic increase in the computed Ω value, as one goes from model A to model B. Due to the high level of correlation between calculation and experiment, and as the crystal structures are known, for BaBr_2 and SrBr_2 , we are able to fully assign the measured $^{79/81}\text{Br}$ SSNMR signals to specific crystallographic sites (see Figure 2 and Table 1 for the labeling scheme used).

B. Calculated Bromine \ddot{V} and $\ddot{\sigma}$ Absolute Tensor Orientations. The relative orientation of the \ddot{V} and $\ddot{\sigma}$ tensor PASs may be measured in powdered samples and, under certain conditions, the absolute orientation may also be inferred.^{147,149} Computational methods generally offer insight regarding the absolute orientation of these PASs. In all the pure samples studied herein, evidence of noncoincident tensor frames was observed and quantified (Tables 1 and 2), and it was observed that $^{79/81}\text{Br}$ SSNMR spectra are sensitive to the β value (i.e., the angular separation between the σ_{33} and V_{33} principal axes).

The local symmetry at the Br ions in CaBr_2 is m , with the mirror plane lying perpendicular to the c crystal axis. As expected, the computed \ddot{V} and (symmetric) $\ddot{\sigma}$ eigenvectors at the Br are either parallel or perpendicular to this mirror plane (Figure 12a). The V_{11} eigenvector orients along c , directly toward a neighboring Br ion. As the EFG magnitude bears a $1/r^3$ (r being the internuclear distance) dependence, and as the bromide–bromide distance along the c axis is greater (4.34 Å) than the corresponding distance parallel to the mirror plane (3.80 Å), the orientation of V_{11} is perhaps unsurprising. The \ddot{V} eigenvalues are similar for the eigenvectors parallel to the mirror plane (hence, the large computed η_Q of 0.496). With regards to bromine magnetic shielding in CaBr_2 , there is no unique

component ($\kappa \sim 0$) and σ_{22} orients perpendicular to the mirror plane. Halogen chemical shifts in ionic systems are largely determined by the degree of ion orbital overlap with its nearest neighbors (NN) and next-nearest neighbors (NNN).¹¹ From the perspective of the Br ions in CaBr_2 , the NN are the three calcium ions, located at essentially the same distance (2.88 to 2.92 Å) and hence the contributions to magnetic shielding from the NN are likely similar. If we look at the NNN, several bromine ions are found between 3.80 to 4.34 Å. Due to this spread in distances, the shielding should be slightly greater in the direction of the shortest NNN interatomic distance. Indeed, σ_{33} is oriented very nearly along (i.e., $< 10^\circ$ away) the shortest Br–Br internuclear vector. There are no proximate bromine ions near the σ_{11} direction, where reduced ion orbital overlap is expected.

There are two magnetically unique Br sites in BaBr_2 . Each possesses local m symmetry, with the mirror plane orienting perpendicular to the b crystal axis. The calculated eigenvector orientations for the \ddot{V} and $\ddot{\sigma}$ tensors at each distinct Br lie either perpendicular or parallel to the mirror plane. Considering Br(1), V_{11} and V_{33} lie parallel to the mirror plane, with V_{22} orienting perpendicular to it (Figure 12b). The V_{33} eigenvector orients very nearly toward the nearest Ba^{2+} ion ($\angle(V_{33}-\text{Br}-\text{Ba}) = 5.8^\circ$), while V_{22} points directly at an adjacent Br ion. The σ_{33} and σ_{11} eigenvectors lie parallel to the mirror plane, with σ_{22} orienting parallel to b . As with CaBr_2 , σ_{33} directs not toward a metal cation but rather roughly toward a somewhat distant ($r = 5.58$ Å) Br(2) atom. Likewise, σ_{22} points along b , directly at the most local bromine in that direction. With regards to the Br(2) sites in BaBr_2 , the \ddot{V} tensor orients very similarly to that for the Br(1) site. In fact, the directions of the V_{22}/σ_{22} eigenvectors are equivalent. The σ_{33} eigenvector for Br(2) nearly bisects the angle that the Br(2) makes with the two most proximate Br(1) ions, while σ_{11} for Br(2) points roughly toward a fairly remote ($r = 5.43$ Å) Br(2) atom.

We will not go into further detail regarding the tensor orientations for all the compounds studied. Considering the \ddot{V} and $\ddot{\sigma}$ tensor orientations across all samples (Figure 12 and

TABLE 5: Calculated ^{81}Br EFG Parameters: Point Charge Model^a

compound	site label	$C_Q(^{81}\text{Br})/\text{MHz}$	η_Q
CaBr ₂	—	-141.6	0.70
SrBr ₂	Br(1)	-10.8	0.00
	Br(2)	-14.8	0.00
	Br(3)	38.8	0.61
	Br(4)	-104.6	0.59
BaBr ₂	Br(1)	-17.6	0.40
	Br(2)	49.8	0.03

^a The following equation was used to calculate the ij th ($i, j = x, y, z$) component of V : $V_{ij} = ((Ze)/(4\pi\epsilon_0 r^3))((3rr_j)/(r^2) - \delta_{ij})$, where Z is the value associated with a point charge (i.e., -1 for Br and +2 for the alkaline earth metal) located a distance r away from the probe nucleus, ϵ_0 is the permittivity of free space, and δ_{ij} is the Kronecker delta function. See also footnote *b* of Table 3.

Supporting Information: Figures S8–S11, and Table S7), beyond simple symmetry constraints it is not straightforward to rationalize their orientation in a general manner. In a number of cases, V_{33} orients toward a nearby M^{2+} ion (e.g., both BaBr₂ sites, the Br(3) and Br(4) sites in SrBr₂), but it is also seen that V_{33} can orient toward a nearby Br⁻ anion (e.g., CaBr₂ and sites Br(1) and Br(2) in SrBr₂). The situation is similar when looking at the orientation of σ_{33} . Among all compounds studied, it appears that the local ions dictate the tensor orientation; hence, the resultant tensors typically possess eigenvectors that are oriented at or near either NN or NNN ions.

3. Calculation of Bromine \ddot{V} Tensors Using a Point Charge Model. To determine the effect of the ionic lattice upon the resultant \ddot{V} tensor at the Br nuclei, calculations using a point charge model¹⁵⁰ were carried out for the anhydrous complexes (Table 5). After the inclusion of Sternheimer antishielding effects, small QIs are reproduced rather well (e.g., Br(1) and Br(2) sites in SrBr₂). For moderate C_Q values (e.g., Br(3) in SrBr₂), the agreement between observation and calculation becomes worse, with the point charge model overestimating the experimental $C_Q(^{81}\text{Br})$ values. Agreement is very poor in cases of a substantial QI (e.g., CaBr₂ or Br(4) in SrBr₂). We postulate that the overestimation is due to reduced ionicity, which would decrease the effective ionic charges at all ion sites and hence reduce bromine C_Q values (see Supporting Information, Figure S12, for a plot demonstrating this relationship within the point charge model). Similarly, there should be increasing point dipole effects,¹⁵¹ which are neglected. It therefore appears that a more sophisticated approach, such as GIPAW DFT, is essential to obtain an accurate bromine \ddot{V} tensor in simple ionic bromide systems that possess significant QIs.

Conclusions

We have presented the first systematic $^{79/81}\text{Br}$ SSNMR study relating $^{79/81}\text{Br}$ EFG and CSA tensor parameters to local structure in noncubic inorganic solids. The large range of values observed for the various parameters, e.g., $C_Q(^{79/81}\text{Br})$ values, clearly demonstrates the sensitivity of such experiments to the notable differences in local structure and symmetry for the bromide-containing systems studied. Advantages over bromine NQR include ease of measurement (i.e., no need for powder samples in gram quantities or large single crystals), the opportunity to observe the full \ddot{V} tensor, and the opportunity to measure chemical shift tensors. Indeed, deficiencies in the ^{79}Br NQR data for BaBr₂ and SrBr₂ have been explained and corrected. Measurement of \ddot{V} and $\ddot{\delta}$ tensors, as well as their relative orientations, has been found generally useful across the samples studied: by quantifying the contributions that each tensor makes

to the observed $^{79/81}\text{Br}$ SSNMR line-shape, local site symmetry can be constrained (e.g., as demonstrated in the case of two of the four Br sites in SrBr₂), or, in favorable situations (either very high or very low site symmetry), it can be unambiguously specified (e.g., the $^{79/81}\text{Br}$ SSNMR data clearly show that the Br ions in BaBr₂·2H₂O must be located at crystal lattice positions possessing 1 site symmetry).

As a result of the state-of-the-art ultrahigh magnetic field used in this study, bromine CSA has been measured in a series of powdered samples for the first time using both NMR-active bromine isotopes. These measurements establish bromine CSA as a new tool for characterizing bromide sites in diverse materials. The resolving power of $^{79/81}\text{Br}$ SSNMR spectroscopy has been established on samples containing up to four magnetically inequivalent sites. Rare examples of $^{79/81}\text{Br}$ MAS NMR spectra have been presented for a sample possessing a noncubic crystal lattice and hence exhibiting second-order quadrupolar line-shape broadening. With the development of MAS probes capable of sample rotation frequencies near 70 kHz,^{152,153} we anticipate additional applications of $^{79/81}\text{Br}$ MAS NMR spectroscopy.

The sensitivity of the bromine chemical shift and C_Q values to the degree of sample hydration has been demonstrated. This sensitivity has been exploited to characterize the composition of CaBr₂· x H₂O. We have shown that the bulk of this mixture is anhydrous CaBr₂, but substantial amounts of the dihydrate and tetrahydrate pseudopolymorphs have also been quantified. Bromine SSNMR thus holds promise for the characterization of unknown solid mixtures containing ionic bromides.

The point charge model, after appropriate Sternheimer corrections, has been found to qualitatively reproduce trends in $C_Q(^{81}\text{Br})$ but is in poor quantitative agreement with many of our experimental observations. For this reason, first-principles calculations are preferable. Agreement between experimentally measured and GIPAW DFT-computed $^{79/81}\text{Br}$ SSNMR parameters has been found to be very good to excellent in most cases. This has allowed for the unambiguous assignment of experimentally observed $^{79/81}\text{Br}$ SSNMR signals to unique sites in the crystal lattices.

On the basis of the range of observed parameters, it appears that $^{79/81}\text{Br}$ SSNMR may be applied as a general spectroscopic tool for the study of bromide-containing systems. The development of larger applied magnetic fields (e.g., Bruker's 1 GHz)¹⁵⁴ and advanced pulse sequences (e.g., WURST-QCPMG and DEISM)^{155,156} will facilitate future studies on more challenging materials. As correctly noted very recently by Alonso et al., bromine SSNMR should be applicable to the study of complex interfaces, such as mesoporous materials.³² Additional opportunities for $^{79/81}\text{Br}$ SSNMR can also be envisioned: molecular systems, such as those containing anion- π interactions;¹⁵⁷ biological systems, such as the bromide mimic of photosystem II (recently shown to have oxygen-evolving capacity);¹⁵⁸ chemical catalysts;¹⁵⁹ and layered photocatalysts, such as BiOBr.¹⁶⁰ Bromine SSNMR could also provide key data in an effort to quantify the role of halogen bonding in supramolecular chemistry.¹⁶¹

Acknowledgment. D.L.B. thanks the Natural Sciences and Engineering Research Council (NSERC) of Canada for funding. C.M.W. thanks NSERC for an Alexander Graham Bell CGS D2 scholarship. Access to the 900 MHz NMR spectrometer was provided by the National Ultrahigh-Field NMR Facility for Solids (Ottawa, Canada), a national research facility funded by the Canada Foundation for Innovation, the Ontario Innovation Trust, Recherche Québec, the National Research Council

Canada, and Bruker BioSpin and is managed by the University of Ottawa (www.nmr900.ca). NSERC is acknowledged for a Major Resources Support grant. Dr. Victor Terskikh, Dr. Glenn Facey, and Dr. Tara Kell are thanked for technical support, and Prof. M. Murugesu (uOttawa) is thanked for the use of his glovebox.

Supporting Information Available: Detailed $^{79/81}\text{Br}$ SS-NMR experimental acquisition parameters; GIPAW DFT computations: energies, structure references, structural parameters used, and additional information; additional SSNMR spectra and analytical simulations: CaBr_2 (^{81}Br QCPMG at 11.75 T and simulations highlighting the effect of Ω and β parameter variation on analytical line-shape simulations), SrBr_2 (highlighting the importance of including both CSA and nonzero Euler angles), $\text{SrBr}_2 \cdot 6\text{H}_2\text{O}$ ($^{79/81}\text{Br}$ Solomon echo spectra at 11.75 T), $\text{CaBr}_2 \cdot x\text{H}_2\text{O}$ (^{81}Br QCPMG spectrum at 11.75 T and $^{79/81}\text{Br}$ Solomon echo spectra of the three central signals at 11.75 and 21.1 T); input parameters for calculations involving isomorphic bromides and chlorides; POV-ray renderings of computed \vec{V} and $\vec{\sigma}$ tensor orientations in the crystal frames of SrBr_2 , $\text{MgBr}_2 \cdot 6\text{H}_2\text{O}$ (model B), $\text{SrBr}_2 \cdot 6\text{H}_2\text{O}$ (model B), $\text{BaBr}_2 \cdot 2\text{H}_2\text{O}$; \vec{V} and $\vec{\sigma}$ tensor eigenvectors, normalized and in their respective crystal frames; plot of $C_Q(\text{Br})$ versus $q(\text{Br})$ for CaBr_2 using the point charge model. This material is available free of charge via the Internet at <http://pubs.acs.org>.

References and Notes

- (1) Cotton, F. A.; Wilkinson, G. *The Group VII Elements: F, Cl, Br, I*, In *Advanced Inorganic Chemistry: A Comprehensive Text*, 4th ed.; Wiley-Interscience: Toronto, 1980; p 546.
- (2) Housecroft, C. E.; Sharpe, A. G. In *Inorganic Chemistry*; Pearson Education Limited: Harlow, England, 2001; p 386.
- (3) Murray, R. W. *Anal. Chem.* **2009**, *81*, 2415.
- (4) Widdifield, C. M.; Bryce, D. L. *Phys. Chem. Chem. Phys.* **2009**, *11*, 7120–7122.
- (5) Widdifield, C. M.; Chapman, R. P.; Bryce, D. L. Chlorine, Bromine, and Iodine Solid-State NMR Spectroscopy In *Annual Reports in NMR Spectroscopy*; Webb, G. A., Ed.; Elsevier: New York, 2009; Vol. 66, pp 195–326.
- (6) Chapman, R. P.; Widdifield, C. M.; Bryce, D. L. *Prog. Nucl. Magn. Reson. Spectrosc.* **2009**, *55*, 215–237.
- (7) Pyyköö, P. *Mol. Phys.* **2008**, *106*, 1965–1974.
- (8) Sternheimer, R. *Phys. Rev.* **1954**, *95*, 736–750.
- (9) Lucken, E. A. C. Sternheimer Shielding In *Nuclear Quadrupole Coupling Constants*; Academic Press: London, 1969; pp 79–96.
- (10) Kanda, T. *J. Phys. Soc. Jpn.* **1955**, *10*, 85–88.
- (11) Yamagata, Y. *J. Phys. Soc. Jpn.* **1964**, *19*, 10–23.
- (12) Wikner, E. G.; Blumberg, W. E.; Hahn, E. L. *Phys. Rev.* **1960**, *118*, 631–639.
- (13) Günther, B. D.; Hultsch, R. A. *J. Magn. Reson.* **1969**, *1*, 609–617.
- (14) Hayashi, S.; Hayamizu, K. *Bull. Chem. Soc. Jpn.* **1990**, *63*, 913–919.
- (15) Hayashi, S.; Hayamizu, K. *J. Chem. Phys.* **1990**, *92*, 2818–2827.
- (16) Hayashi, S.; Hayamizu, K. *J. Phys. Chem. Solids* **1992**, *53*, 239–248.
- (17) Tarasov, V. P.; Petrushin, S. A.; Gusev, Y. K. *Dokl. Akad. Nauk SSSR* **1987**, *293*, 1423–1426.
- (18) Tarasov, V. P.; Petrushin, S. A.; Gusev, Y. K. *Russ. J. Inorg. Chem.* **1988**, *33*, 452–454.
- (19) Tarasov, V. P.; Privalov, V. I.; Gavrichev, K. S.; Gorbunov, V. E.; Gusev, Y. K.; Buslaev, Y. A. *Russ. J. Coord. Chem.* **1990**, *16*, 854–861.
- (20) Tarasov, V. P.; Privalov, V. I.; Buslaev, Y. A.; Eichhoff, U. Z. *Naturforsch. B* **1990**, *45*, 1005–1009.
- (21) Bastow, T. J.; Stuart, S. N.; McDugle, W. G.; Eachus, R. S.; Spaeth, J. M. *J. Phys.: Condens. Matter* **1994**, *6*, 8633–8644.
- (22) Trill, H.; Eckert, H.; Srđanov, V. I. *J. Am. Chem. Soc.* **2002**, *124*, 8361–8370.
- (23) Trill, H.; Eckert, H.; Srđanov, V. I. *J. Phys. Chem. B* **2003**, *107*, 8779–8788.
- (24) Jelinek, R.; Chmelka, B. F.; Stein, A.; Ozin, G. A. Multinuclear Solid-State NMR Study of a Sodalite Semiconductor In *Materials Research Society Symposium Proceedings*, San Francisco, CA, 1992; Vol. 272, p 235.
- (25) Jelinek, R.; Stein, A.; Ozin, G. A. *J. Am. Chem. Soc.* **1993**, *115*, 2390–2396.
- (26) Brinkmann, D.; Huber, H.; Mali, M.; Roos, J.; Arend, H. *Helv. Phys. Acta* **1982**, *55*, 568.
- (27) Brenni, P.; Brinkmann, D.; Huber, H.; Mali, M.; Roos, J.; Arend, H. *Solid State Commun.* **1983**, *47*, 415–418.
- (28) Erge, T.; Michel, D.; Petersson, J.; Engelke, F. *Phys. Status Solidi A* **1991**, *123*, 325–331.
- (29) Michel, D.; Häcker, U.; Erge, T.; Petersson, J. *Phys. Status Solidi B* **1994**, *185*, 257–264.
- (30) Kehrer, A.; Weiden, N.; Weiss, A. *Z. Phys. Chem.* **1992**, *178*, 1–24.
- (31) Persons, J.; Harbison, G. S. *J. Magn. Reson.* **2007**, *186*, 347–351.
- (32) Alonso, B.; Massiot, D.; Florian, P.; Paradies, H. H.; Gaveau, P.; Mineva, T. *J. Phys. Chem. B* **2009**, *113*, 11906–11920.
- (33) Bryce, D. L.; Sward, G. D. *Magn. Reson. Chem.* **2006**, *44*, 409–450.
- (34) Kentgens, A. P. M.; Verhagen, R. *Chem. Phys. Lett.* **1999**, *300*, 435–443.
- (35) Yao, Z.; Kwak, H. T.; Sakellariou, D.; Emsley, L.; Grandinetti, P. *J. Chem. Phys. Lett.* **2000**, *327*, 85–90.
- (36) Siegel, R.; Nakashima, T. T.; Wasylisen, R. E. *Chem. Phys. Lett.* **2004**, *388*, 441–445.
- (37) Schurko, R. W.; Hung, I.; Widdifield, C. M. *Chem. Phys. Lett.* **2003**, *379*, 1–10.
- (38) Siegel, R.; Nakashima, T. T.; Wasylisen, R. E. *Concepts Magn. Reson. A* **2005**, *26*, 47–61.
- (39) Larsen, F. H.; Jakobsen, H. J.; Ellis, P. D.; Nielsen, N. C. *J. Phys. Chem. A* **1997**, *101*, 8597–8606.
- (40) Siegel, R.; Nakashima, T. T.; Wasylisen, R. E. *Concepts Magn. Reson. A* **2005**, *26*, 62–77.
- (41) O'Dell, L. A.; Schurko, R. W. *Chem. Phys. Lett.* **2008**, *464*, 97–102.
- (42) Weeding, T. L.; Veeman, W. S. *J. Chem. Soc., Chem. Commun.* **1989**, 946–948.
- (43) Jurga, S.; Harbison, G. S.; Blümich, B.; Spiess, H. W.; Fujara, F.; Olinger, A. *Ber. Bunsen-Ges. Phys. Chem.* **1986**, *90*, 1153–1159.
- (44) Segel, S. L.; Maxwell, S.; Heyding, R. D.; Ingman, P.; Ylinen, E.; Punkkinen, M. *Solid State Commun.* **1988**, *66*, 1039–1041.
- (45) Bastow, T. J.; Brown, R. J. C.; Segel, S. L. *J. Chem. Phys.* **1988**, *89*, 1203–1204.
- (46) Bastow, T. J.; Stuart, S. N. *J. Phys.: Condens. Matter* **1989**, *1*, 4649–4657.
- (47) Tarasov, V. P.; Meladze, M. A.; Kirakosyan, G. A.; Shvelashvili, A. E.; Buslaev, Y. A. *Phys. Status Solidi B* **1991**, *167*, 271–279.
- (48) Tarasov, V. P.; Meladze, M. A.; Kirakosyan, G. A. *Russ. J. Coord. Chem.* **1992**, *18*, 707–717.
- (49) Furukawa, Y.; Ikeda, R. *Ber. Bunsen-Ges. Phys. Chem.* **1993**, *97*, 1143–1146.
- (50) Skibsted, J.; Jakobsen, H. J. *Inorg. Chem.* **1999**, *38*, 1806–1813.
- (51) Gervais, C.; Dupree, R.; Pike, K. J.; Bonhomme, C.; Profeta, M.; Pickard, C. J.; Mauri, F. *J. Phys. Chem. A* **2005**, *109*, 6960–6969.
- (52) Bryce, D. L.; Sward, G. D.; Adiga, S. *J. Am. Chem. Soc.* **2006**, *128*, 2121–2134.
- (53) Bryce, D. L.; Sward, G. D. *J. Phys. Chem. B* **2006**, *110*, 26461–26470.
- (54) Chapman, R. P.; Bryce, D. L. *Phys. Chem. Chem. Phys.* **2007**, *9*, 6219–6230.
- (55) Sandland, T. O.; Du, L. S.; Stebbins, J. F.; Webster, J. D. *Geochim. Cosmochim. Acta* **2004**, *68*, 5059–5069.
- (56) Bryce, D. L.; Bultz, E. B. *Chem.—Eur. J.* **2007**, *13*, 4786–4796.
- (57) Hamaed, H.; Pawłowski, J. M.; Cooper, B. F. T.; Fu, R.; Eichhorn, S. H.; Schurko, R. W. *J. Am. Chem. Soc.* **2008**, *130*, 11056–11065.
- (58) Rossini, A. J.; Mills, R. W.; Briscoe, G. A.; Norton, E. L.; Geier, S. J.; Hung, I.; Zheng, S.; Autschbach, J.; Schurko, R. W. *J. Am. Chem. Soc.* **2009**, *131*, 3317–3330.
- (59) Gordon, P. G.; Brouwer, D. H.; Ripmeester, J. A. *J. Phys. Chem. A* **2008**, *112*, 12527–12529.
- (60) Liang, H.; Hanzawa, H.; Horikawa, T.; Machida, K. *J. Alloys Compd.* **2008**, *457*, L6–L8.
- (61) Temelkov, K. A.; Vuchkov, N. K.; Pan, B. L.; Sabotinov, N. V.; Ivanov, B.; Lyutov, L. *J. Phys. D: Appl. Phys.* **2006**, *39*, 3769–3772.
- (62) Iwase, N.; Tadaki, S.; Hidaka, S.; Koshino, N. *J. Lumin.* **1994**, *60&61*, 618–619.
- (63) Corradi, G.; Secu, M.; Schweizer, S.; Spaeth, J. M. *J. Phys.: Condens. Matter* **2004**, *16*, 1489–1500.
- (64) Selling, J.; Birowosuto, M. D.; Dorenbos, P.; Schweizer, S. *J. Appl. Phys.* **2007**, *101*, 034901.
- (65) Selling, J.; Schweizer, S.; Birowosuto, M. D.; Dorenbos, P. *J. Appl. Phys.* **2007**, *102*, 074915.
- (66) Eichele, K.; Wasylisen, R. E. WSolids NMR Simulation Package, 2001, v.1.17.30.

- (67) Herzfeld, J.; Berger, A. E. *J. Chem. Phys.* **1980**, *73*, 6021–6030.
 (68) Mason, J. *Solid State Nucl. Magn. Reson.* **1993**, *2*, 285–288.
 (69) Jameson, C. J. *Solid State Nucl. Magn. Reson.* **1998**, *11*, 265–268.
 (70) Bryce, D. L. *Tensor Interplay In NMR Crystallography*; Harris, R. K., Wasylisen, R. E., Duer, M. J., Eds.; John Wiley and Sons Ltd.: Chichester, 2009; pp 289–301.
 (71) Tanaka, H. *Thermochim. Acta* **1985**, *90*, 101–107.
 (72) Solomon, I. *Phys. Rev.* **1958**, *110*, 61–65.
 (73) Weisman, I. D.; Bennett, L. H. *Phys. Rev.* **1969**, *181*, 1341–1350.
 (74) Kunwar, A. C.; Turner, G. L.; Oldfield, E. *J. Magn. Reson.* **1986**, *69*, 124–127.
 (75) Carr, H. Y.; Purcell, E. M. *Phys. Rev.* **1954**, *94*, 630–638.
 (76) Meiboom, S.; Gill, D. *Rev. Sci. Instrum.* **1958**, *29*, 688–691.
 (77) Massiot, D.; Farnan, I.; Gautier, N.; Trumeau, D.; Trokiner, A.; Coutures, J. P. *Solid State Nucl. Magn. Reson.* **1995**, *4*, 241–248.
 (78) Medek, A.; Frydman, V.; Frydman, L. *J. Phys. Chem. A* **1999**, *103*, 4830–4835.
 (79) Schurko, R. W.; Wi, S.; Frydman, L. *J. Phys. Chem. A* **2002**, *106*, 51–62.
 (80) Pickard, C. J.; Mauri, F. *Phys. Rev. B* **2001**, *63*, 245101.
 (81) Yates, J. R.; Pickard, C. J.; Mauri, F. *Phys. Rev. B* **2007**, *76*, 024401.
 (82) Profeta, M.; Mauri, F.; Pickard, C. J. *J. Am. Chem. Soc.* **2003**, *125*, 541–548.
 (83) Clark, S. J.; Segall, M. D.; Pickard, C. J.; Hasnip, P. J.; Probert, M. I. J.; Refson, K.; Payne, M. C. Z. *Kristallogr.* **2005**, *220*, 567.
 (84) Perdew, J. P.; Burke, K.; Ernzerhof, M. *Phys. Rev. Lett.* **1996**, *77*, 3865–3868.
 (85) Perdew, J. P.; Burke, K.; Ernzerhof, M. *Phys. Rev. Lett.* **1997**, *78*, 1396.
 (86) Burke, K.; Perdew, J. P.; Wang, Y. In *Electronic Density Functional Theory: Recent Progress and New Directions*; Dobson, J. F., Vignale, G., Das, M. P., Eds.; Plenum: New York, 1998.
 (87) Perdew, J. P. In *Electronic Structure of Solids '91*; Ziesche, P., Eschrig, H., Eds.; Akademie Verlag: Berlin, 1991; p 11.
 (88) Perdew, J. P.; Chevary, J. A.; Vosko, S. H.; Jackson, K. A.; Pederson, M. R.; Singh, D. J.; Fiolhais, C. *Phys. Rev. B* **1992**, *46*, 6671–6687.
 (89) Perdew, J. P.; Chevary, J. A.; Vosko, S. H.; Jackson, K. A.; Pederson, M. R.; Singh, D. J.; Fiolhais, C. *Phys. Rev. B* **1993**, *48*, 4978.
 (90) Perdew, J. P.; Burke, K.; Wang, Y. *Phys. Rev. B* **1996**, *54*, 16533–16539.
 (91) Monkhorst, H. J.; Pack, J. D. *Phys. Rev. B* **1976**, *13*, 5188–5192.
 (92) Andress, K. R.; Gundermann, J. Z. *Kristallogr.* **1934**, *87*, 345–369.
 (93) Sorrell, C. A.; Ramey, R. R. *J. Chem. Eng. Data* **1974**, *19*, 307–308.
 (94) Abrahams, I.; Vordemvenne, E. *Acta Crystallogr., Sect. C: Cryst. Struct. Commun.* **1995**, *C51*, 183–185.
 (95) Agron, P. A.; Busing, W. R. *Acta Crystallogr., Sect. C: Cryst. Struct. Commun.* **1986**, *C42*, 141–143.
 (96) LeClaire, A.; Borel, M. M. *Acta Crystallogr., Sect. B: Struct. Crystallogr. Cryst. Chem.* **1977**, *B33*, 2938–2940.
 (97) MacKenzie, K. J. D.; Smith, M. E. *Multinuclear Solid-State NMR of Inorganic Materials*; Pergamon: Amsterdam, 2002.
 (98) Abragam, A. *Principles of Nuclear Magnetism*; Oxford University Press: New York, 1961.
 (99) van Bever, A. K.; Nieuwenkamp, W. Z. *Kristallogr.* **1935**, *90*, 374–376.
 (100) Döll, V. W.; Klemm, W. Z. *Anorg. Allg. Chem.* **1939**, *241*, 239–258.
 (101) Brackett, E. B.; Brackett, T. E.; Sass, R. L. *J. Inorg. Nucl. Chem.* **1963**, *25*, 1295–1296.
 (102) Bondi, A. *J. Phys. Chem.* **1964**, *68*, 441–451.
 (103) Mantina, M.; Chamberlin, A. C.; Valero, R.; Cramer, C. J.; Truhlar, D. G. *J. Phys. Chem. A* **2009**, *113*, 5806–5812.
 (104) Lin, Z.; Smith, M. E.; Sowrey, F. E.; Newport, R. *J. Phys. Rev. B* **2004**, *69*, 224107.
 (105) Smirnov, N. I.; Volkov, A. F. *Teor. Eksp. Khim.* **1976**, *13*, 88–90.
 (106) Lucken, E. A. C. *Nuclear Quadrupole Coupling Constants*; Academic Press: London, 1969.
 (107) Bain, A. D. *Mol. Phys.* **2003**, *101*, 3163–3175.
 (108) Wu, G.; Terskikh, V. *J. Phys. Chem. A* **2008**, *112*, 10359–10364.
 (109) Fusaro, R.; Doane, J. W. *J. Chem. Phys.* **1967**, *47*, 5446–5447.
 (110) Kamermans, M. A. Z. *Kristallogr.* **1939**, *101*, 406–411.
 (111) Sass, R. L.; Brackett, T.; Brackett, E. *J. Phys. Chem.* **1963**, *67*, 2862–2863.
 (112) Smeggil, J. G.; Eick, H. A. *Inorg. Chem.* **1971**, *10*, 1458–1460.
 (113) Buckingham, A. D.; Malm, S. M. *Mol. Phys.* **1971**, *22*, 1127–1130.
 (114) Hou, X.; Kirkpatrick, R. J. *Chem. Mater.* **2002**, *14*, 1195–1200.
 (115) Brackett, E. B.; Brackett, T. E.; Sass, R. L. *J. Phys. Chem.* **1963**, *67*, 2132–2135.
 (116) Volkov, A. F.; Smirnov, N. I. *Dokl. Akad. Nauk SSSR* **1973**, *211*, 1377–1379.
 (117) Potrepka, D. M.; Budnick, J. I.; Fenner, D. B.; Hines, W. A.; Balasubramanian, M.; Moodenbaugh, A. R. *Phys. Rev. B* **1999**, *60*, 10489–10499.
 (118) Stebbins, J. F.; Du, L. S. *Am. Mineral.* **2002**, *87*, 359–363.
 (119) Bang, E. *Mat. Fys. Medd. Dan. Vid. Selsk.* **1961**, *33*, 1–23.
 (120) Lutz, H. D.; Engelen, B.; Freiburg, C. *Acta Crystallogr., Sect. B: Struct. Crystallogr. Cryst. Chem.* **1980**, *B36*, 437–438.
 (121) Kellersohn, T.; Engelen, B.; Lutz, H. D.; Bartl, H.; Schweiss, B. P.; Fuess, H. Z. *Kristallogr.* **1991**, *197*, 175–184.
 (122) McGrath, J. W.; Silvidi, A. A. *J. Chem. Phys.* **1960**, *33*, 644–647.
 (123) McGrath, J. W.; Silvidi, A. A. *J. Chem. Phys.* **1962**, *36*, 1082.
 (124) McGrath, J. W.; Silvidi, A. A. *J. Chem. Phys.* **1962**, *37*, 194–195.
 (125) McGrath, J. W. *J. Chem. Phys.* **1965**, *43*, 3746–3749.
 (126) Silvidi, A. A. *J. Chem. Phys.* **1966**, *45*, 3892–3894.
 (127) van der Elsken, J.; Robinson, D. W. *Spectrochim. Acta* **1961**, *17*, 1249–1256.
 (128) Hanawalt, J. D.; Rinn, H. W.; Frevel, L. K. *Ind. Eng. Chem., Anal. Ed.* **1938**, *10*, 457–512.
 (129) Agron, P. A.; Busing, W. R. *Acta Crystallogr., Sect. C: Cryst. Struct. Commun.* **1985**, *C41*, 8–10.
 (130) Hiyama, Y.; Woyciesjes, P. M.; Brown, T. L.; Torchia, D. A. *J. Magn. Reson.* **1987**, *72*, 1–12.
 (131) Sidei, T.; Yano, S. *J. Chem. Phys.* **1955**, *23*, 1554–1555.
 (132) Herrmann, Z. Z. *Anorg. Allg. Chem.* **1931**, *196*, 79–84.
 (133) Yano, S. *J. Phys. Soc. Jpn.* **1959**, *14*, 942–954.
 (134) Paulik, J.; Paulik, F.; Buzágh-Gere, É.; Arnold, M. *Thermochim. Acta* **1979**, *31*, 93–100.
 (135) Trouillier, N.; Martins, J. L. *Phys. Rev. B* **1991**, *43*, 1993–2006.
 (136) Vanderbilt, D. *Phys. Rev. B* **1990**, *41*, 7892–7895.
 (137) Mauri, F.; Vast, N.; Pickard, C. J. *Phys. Rev. Lett.* **2001**, *87*, 085506.
 (138) Farnan, I.; Balan, E.; Pickard, C. J.; Mauri, F. *Am. Mineral.* **2003**, *88*, 1663–1667.
 (139) Gervais, C.; Profeta, M.; Lafond, V.; Bonhomme, C.; Azaïs, T.; Mutin, H.; Pickard, C. J.; Mauri, F.; Babonneau, F. *Magn. Reson. Chem.* **2004**, *42*, 445–452.
 (140) Bouchmella, K.; Dutremez, S. G.; Alonso, B.; Mauri, F.; Gervais, C. *Cryst. Growth Des.* **2008**, *8*, 3941–3950.
 (141) Blöchl, P. E. *Phys. Rev. B* **1994**, *50*, 17953–17979.
 (142) Zwanziger, J. W.; Torrent, M. *Appl. Magn. Reson.* **2008**, *33*, 447–456.
 (143) Charpentier, T.; Ispas, S.; Profeta, M.; Mauri, F.; Pickard, C. J. *J. Phys. Chem. B* **2004**, *108*, 4147–4161.
 (144) Profeta, M.; Benoit, M.; Mauri, F.; Pickard, C. J. *J. Am. Chem. Soc.* **2004**, *126*, 12628–12635.
 (145) Choi, M.; Matsunaga, K.; Oba, F.; Tanaka, I. *J. Phys. Chem. C* **2009**, *113*, 3869–3873.
 (146) Gervais, C.; Laurencin, D.; Wong, A.; Pourpoint, F.; Labram, J.; Woodward, B.; Howes, A. P.; Pike, K. J.; Dupree, R.; Mauri, F.; Bonhomme, C.; Smith, M. E. *Chem. Phys. Lett.* **2008**, *464*, 42–48.
 (147) Bryce, D. L.; Bultz, E. B.; Aebi, D. *J. Am. Chem. Soc.* **2008**, *130*, 9282–9292.
 (148) Jameson, C. J.; de Dios, A. C. Theoretical and physical aspects of nuclear shielding In *Nuclear Magnetic Resonance*; Webb, G. A., Ed.; RSC Publishing: Dorchester, 2009; Vol. 38, pp 68–93.
 (149) Edén, M. *Chem. Phys. Lett.* **2009**, *470*, 318–324.
 (150) Slichter, C. P. *Principles of Magnetic Resonance*; Springer-Verlag: New York, 1990.
 (151) Han, O. H.; Oldfield, E. *Inorg. Chem.* **1990**, *29*, 3666–3669.
 (152) Samoson, A.; Tuherm, T.; Gan, Z. *Solid State Nucl. Magn. Reson.* **2001**, *20*, 130–136.
 (153) Samoson, A.; Tuherm, T.; Past, J.; Reinhold, A.; Anupöld, T.; Heinmaa, I. *Top. Curr. Chem.* **2005**, *246*, 15–31.
 (154) Bruker Announces AVANCE 1000, the World's First 1 Gigahertz NMR Spectrometer. <http://www.bruker-biospin.com/pr090601.html> (accessed Sep 18, 2009).
 (155) O'Dell, L. A.; Rossini, A. J.; Schurko, R. W. *Chem. Phys. Lett.* **2009**, *468*, 330–335.
 (156) O'Dell, L. A.; Schurko, R. W. *J. Am. Chem. Soc.* **2009**, *131*, 6658–6659.
 (157) Hay, B. P.; Custelcean, R. *Cryst. Growth Des.* **2009**, *9*, 2539–2545.
 (158) Kawakami, K.; Umena, Y.; Kamiya, N.; Shen, J. R. *Proc. Natl. Acad. Sci. U.S.A.* **2009**, *106*, 8567–8572.
 (159) Zhao, Y. J.; Tan, L. J. S.; Li, B.; Li, S. M.; Loh, T. P. *Chem. Commun.* **2009**, 3738–3740.
 (160) Huang, W. L. *J. Comput. Chem.* **2009**, *30*, 1882–1891.
 (161) Metrangolo, P.; Meyer, F.; Pilati, T.; Resnati, G.; Terraneo, G. *Angew. Chem., Int. Ed.* **2008**, *47*, 6114–6127.